Bending and free vibrations of functionally graded annular and circular micro-plates under thermal loading

Iman Eshraghi, Serkan Dag, Nasser Soltani

PII: S0263-8223(15)01014-4
DOI: http://dx.doi.org/10.1016/j.compstruct.2015.11.024
Reference: COST 6979

To appear in: *Composite Structures*

Please cite this article as: Eshraghi, I., Dag, S., Soltani, N., Bending and free vibrations of functionally graded annular and circular micro-plates under thermal loading, *Composite Structures* (2015), doi: http://dx.doi.org/10.1016/j.compstruct.2015.11.024

Bending and free vibrations of functionally graded annular and circular micro-plates under thermal loading

Iman Eshraghi [a], Serkan Dag [b,*], Nasser Soltani [a]

[a] *School of Mechanical Engineering, College of Engineering, University of Tehran, Tehran, Iran*
[b] *Department of Mechanical Engineering, Middle East Technical University, Ankara 06800, Turkey*

ABSTRACT

We introduce solution methods capable of treating static bending and free vibration problems involving thermally loaded functionally graded annular and circular micro-plates. Formulation is based on modified couple stress theory; and related governing partial differential equations and boundary conditions are derived by means of Hamilton's principle. Displacement field is expressed in a unified way so as to produce numerical results in accordance with Kirchhoff, Mindlin, and third-order shear deformation theories. All material properties, including the length scale parameter, are assumed to be functions of the thickness coordinate. The static and dynamic problems are solved by means of differential quadrature method. Proposed procedures are verified through comparisons made to the findings available in the technical literature on thermally stressed axisymmetric plates. Detailed numerical results are presented in order to demonstrate the influences of thermal loading magnitude, and material and geometric parameters upon static deformation profiles, stresses, and natural vibration frequencies.

Keywords: Functionally graded materials; annular and circular micro-plates; modified couple stress theory; bending; free vibrations; thermal loading.

* Corresponding author. Tel.: +90-312-2102580; fax: +90-312-2102536.
E-mail address: sdag@metu.edu.tr (Serkan Dag).

1. Introduction

Functionally graded materials (FGMs) are advanced composites, that possess smooth spatial variations in the volume fractions of the constituent phases. These variations are additional degrees of freedom in materials design and allow customization of physical properties. The characteristic feature of FGMs is inhomogeneity at both micro- and macro-scale. The inhomogeneity and continuous spatial variations of the physical properties need to be accounted for in theoretical and computational studies so as to produce realistic results regarding behavior of graded structures.

Since the inception of the concept, FGMs have been proposed to be employed in a number of technological applications such as thermal barrier and tribological coatings [1,2], biomaterials [3,4], and solid oxide fuel cells [5]. In recent years, use of functionally graded structures in micro-electro-mechanical-systems (MEMS) also became feasible with the introduction of micro-scale FGM component production techniques like magnetron sputtering [6], plasma-enhanced chemical vapor deposition [7], and modified soft lithography [8]. As a result, there have been extensive research efforts directed towards examining mechanical behavior of micro-scale functionally graded structures. An important group of such structural members is comprised of micro-plates. Annular, circular, and rectangular micro-plates find applications in MEMS including micro-scale resonators, optical and pressure sensors, and gear pumps [9-12]. Our main objective in the present study is to develop methods of analysis for functionally graded *annular and circular* micro-plates, that are under the influence of *thermal loading*.

Modeling and analysis of micro-scale structures require adoption of an higher order continuum theory, that takes into account the size effect. The most commonly used higher order continuum theory in the analysis of annular and circular micro-plates is modified couple stress theory [13]. A single length scale parameter is needed in this theory to describe material

response at the micro-scale. Modified couple stress theory based previous work on annular and circular micro-plates encompass both homogeneous and functionally graded structures. Wang et al. [14] and Zhou and Gao [15] presented procedures capable of resolving static bending problems involving homogeneous circular micro-plates. Results regarding large amplitude free vibrations of homogeneous circular plates are provided by Wang et al. [16]. In articles on functionally graded annular and circular micro-plates, examined problems include bending [17-19], free vibrations [17,18,20], buckling [18], and post-buckling [21].

The articles mentioned in the foregoing paragraph do not take thermal effects into consideration. Thermal loads on micro-scale structures could be induced due to environmental or electrical effects. Depending on the constraints imposed on the micro-structure, these loads may lead to severe thermal stresses that could jeopardize structural integrity. Thus, in analysis and design, it is important to possess tools capable of considering thermal loads acting on micro-scale structures. In the present article, we put forward modified couple stress theory based solutions for *thermally loaded* functionally graded annular and circular micro-plates. Presented techniques are capable of resolving static bending and free vibration problems by taking into account through-the-thickness temperature variation and thermal strains.

The main advantage of modified couple stress theory over other higher order continuum theories is that, it requires a single material property for micro-scale material characterization. This property is the length scale parameter, which can be determined through experimental procedures as described by Lam et al. [22]. Strain gradient elasticity theory, which is another commonly used higher order continuum theory, requires three additional material properties in the characterization [22]. Hence, modified couple stress theory is simpler to implement, and capable of successfully capturing the size effect prevailing at the micro-scale.

The posed static and dynamic problems are formulated in terms of partial differential equations. Two sets of governing partial differential equations are derived for *thermally*

loaded FGM annular and circular micro-plates. One group of equations is valid for micro-plates in static bending and the other is applicable for micro-plates undergoing free vibrations. A unified formulation is established to be able generate results for three different plate theories, namely Kirchhoff plate theory (KPT), Mindlin plate theory (MPT), and third-order shear deformation plate theory (TSDT). The systems comprising governing equations and boundary conditions are solved numerically by means of differential quadrature method (DQM). Proposed techniques are verified by making comparisons to the findings available in the literature. Presented numerical results shed light on the influences of thermal loading, and material and geometric parameters upon static deformation profiles, stresses, and natural vibration frequencies.

2. Formulation

Fig. 1 depicts a functionally graded annular micro-plate, that is assumed to be under the influence of thermal loading. Inner and outer radii, and thickness of the plate are respectively denoted by R_i, R_o, and h. Circular micro-plate possesses exactly the same geometric features except for the fact that $R_i = 0$. All material properties and temperature are functions of only the thickness coordinate, i.e. z. As a consequence, temperature and deformation fields are both axisymmetric.

Ceramic-metal functionally graded annular and circular micro-plates are considered in the parametric analyses. All plates are 100% metallic at $z = -h/2$ and 100% ceramic at $z = h/2$. In the computation of elastic properties modulus of elasticity and Poisson's ratio, we utilize Mori-Tanaka method [23]. These two properties are of the forms

$$E(z) = \frac{9B_e(z)\mu_e(z)}{3B_e(z) + \mu_e(z)}, \tag{1a}$$

$$\nu(z)=\frac{3B_e(z)-2\mu_e(z)}{6B_e(z)+2\mu_e(z)}, \tag{1b}$$

$$B_e=\frac{V_c(B_c-B_m)}{1+\dfrac{(B_c-B_m)V_m}{\dfrac{4\mu_m}{3}+B_m}}+B_m, \qquad \mu_e=\frac{V_c(\mu_c-\mu_m)}{1+\dfrac{(\mu_c-\mu_m)V_m}{\left\{\mu_m+\dfrac{(9B_m+8\mu_m)\mu_m}{6(B_m+2\mu_m)}\right\}}}+\mu_m. \tag{1c}$$

E, ν, B_e, μ_e, and V here respectively designate modulus of elasticity, Poisson's ratio, effective bulk modulus, effective shear modulus, and volume fraction. The subscripts *c* and *m* stand for ceramic and metallic phases. Volume fractions are written in terms of a power function as follows:

$$V_c(z)=\left(\frac{1}{2}+\frac{z}{h}\right)^{\lambda}, \tag{2a}$$

$$V_m(z)=1-V_c(z), \tag{2b}$$

where λ is an inhomogeneity parameter. Mass density, length scale parameter, thermal conductivity, and thermal expansion coefficient variations are evaluated employing rule of mixtures and respectively expressed as:

$$\rho(z)=\rho_c V_c(z)+\rho_m V_m(z), \tag{3a}$$

$$l(z)=l_c V_c(z)+l_m V_m(z), \tag{3b}$$

$$k(z)=k_c V_c(z)+k_m V_m(z), \tag{3c}$$

$$\alpha(z)=\alpha_c V_c(z)+\alpha_m V_m(z). \tag{3d}$$

Computation of spatial variation of a physical property of a functionally graded material requires the use of either a micromechanics model or experimental characterization data. In the absence of such theoretical and experimental results, approximate representations are utilized to evaluate material properties. Exponential [24, 25] and power functions [26, 27] are commonly employed to directly represent property variations. Another commonly used approximation involves expressing material properties by means of rule of mixtures. Variations of elastic properties such as modulus of elasticity, Poisson's ratio, and Lame's parameters; and thermal properties like thermal expansion coefficient, and thermal conductivity were evaluated by rule of mixtures in previous studies [28-32]. Due to lack of micromechanics formulations and experimental data, we employed the rule of mixtures representations given in Eq. (3) to approximate the spatial variations.

In the analysis of both static bending and free vibration problems, we suppose that the micro-plate shown in Fig. 1 is subjected to a temperature difference defined by

$$\theta(z) = T(z) - T_o, \tag{4}$$

in which T is final temperature, and T_o is temperature of the stress-free state. Solution of the one-dimensional heat equation for the FGM micro-plate results in the following expression for the temperature distribution

$$\theta(z) = \theta_L + \frac{\theta_U - \theta_L}{\int_{-h/2}^{h/2} \frac{dz}{k(z)}} \int_{-h/2}^{z} \frac{dz}{k(z)}, \tag{5}$$

where $\theta_U = T(h/2) - T_o$, $\theta_L = T(-h/2) - T_o$.

2.1. Formulation for static bending

According to modified couple stress theory [13], constitutive relations are given by:

$$\sigma_{ij} = 2\mu\left(\varepsilon_{ij} - \alpha\theta\delta_{ij}\right) + \lambda\delta_{ij}\left(\varepsilon_{kk} - 3\alpha\theta\right), \tag{6a}$$

$$m_{ij} = 2\mu l^2 \chi_{ij}, \tag{6b}$$

where σ_{ij} is Cauchy stress, ε_{ij} is total strain, μ and λ are Lame parameters, m_{ij} denotes deviatoric part of the couple stress tensor, and χ_{ij} is symmetric curvature tensor. The material properties μ, λ, α, and l are all functions of the thickness coordinate z. ε_{ij} and χ_{ij} are of the forms

$$\boldsymbol{\varepsilon} = \frac{1}{2}\left[\nabla\mathbf{u} + (\nabla\mathbf{u})^{\mathrm{T}}\right], \tag{7a}$$

$$\boldsymbol{\chi} = \frac{1}{2}\left[\nabla\boldsymbol{\omega} + (\nabla\boldsymbol{\omega})^{\mathrm{T}}\right]. \tag{7b}$$

$\mathbf{u}$ and $\boldsymbol{\omega}$ here are respectively displacement and rotation vectors. Displacement vector components are expressed in the following way:

$$u_r(r,z,t) = u(r,t) - z\frac{\partial w}{\partial r} + f(z)\gamma(r,t), \tag{8a}$$

$$u_\theta(r,z,t) = 0, \tag{8b}$$

$$u_z(r,z,t) = w(r,t), \tag{8c}$$

where

$$\gamma(r,t)=\frac{\partial w}{\partial r}-\phi(r,t), \tag{9}$$

ϕ being the rotation at the mid-plane. The function f in Eq. (8a) depends on the plate theory used to represent plate deformation and is defined as:

$$f(z)=\begin{cases} 0, & \text{for Kirchhoff plate theory (KPT)},\\ z, & \text{for Mindlin plate theory (MPT)},\\ z\left(1-\dfrac{4z^2}{3h^2}\right), & \text{for third - order shear deformation theory (TSDT)}. \end{cases} \tag{10}$$

Governing equations and corresponding boundary conditions are derived by means of Hamilton's principle, which for a static problem postulates that

$$\delta U=0, \tag{11}$$

where U is strain energy evaluated from

$$U=\frac{1}{2}\int_{-h/2}^{h/2}\int_{R_i}^{R_o}\{\sigma_{rr}(\varepsilon_{rr}-\alpha\theta)+\sigma_{\theta\theta}(\varepsilon_{\theta\theta}-\alpha\theta)+2(\sigma_{rz}\varepsilon_{rz}+m_{r\theta}\chi_{r\theta}+m_{z\theta}\chi_{z\theta})\}2\pi r\,drdz. \tag{12}$$

Using Eqs. (6)-(10) in conjunction with Eqs. (11) and (12), we derive governing partial differential equations as follows:

$$(F_{11}-B_{11})\left\{\frac{\partial^3 w}{\partial r^3}+\frac{1}{r}\frac{\partial^2 w}{\partial r^2}-\frac{1}{r^2}\frac{\partial w}{\partial r}\right\}+A_{11}\left\{\frac{\partial^2 u}{\partial r^2}+\frac{1}{r}\frac{\partial u}{\partial r}-\frac{u}{r^2}\right\}-F_{11}\left\{\frac{\partial^2 \phi}{\partial r^2}+\frac{1}{r}\frac{\partial \phi}{\partial r}-\frac{\phi}{r^2}\right\}=0, \tag{13a}$$

$$\left\{2F_{22}-D_{11}-F_{33}-A_{552}+F_{572}-\frac{F_{552}}{4}\right\}\left\{r\frac{\partial^4 w}{\partial r^4}+2\frac{\partial^3 w}{\partial r^3}-\frac{1}{r}\frac{\partial^2 w}{\partial r^2}+\frac{1}{r^2}\frac{\partial w}{\partial r}\right\}$$

$$+\left\{\frac{F_{662}}{4}+k_s F_{55}\right\}\left\{r\frac{\partial^2 w}{\partial r^2}+\frac{\partial w}{\partial r}\right\}+\left(B_{11}-F_{11}\right)\left\{r\frac{\partial^3 u}{\partial r^3}+2\frac{\partial^2 u}{\partial r^2}-\frac{1}{r}\frac{\partial u}{\partial r}+\frac{u}{r^2}\right\}$$

$$+\left\{F_{33}-F_{22}-\frac{F_{572}}{2}+\frac{F_{552}}{4}\right\}\left\{r\frac{\partial^3 \phi}{\partial r^3}+2\frac{\partial^2 \phi}{\partial r^2}-\frac{1}{r}\frac{\partial \phi}{\partial r}+\frac{\phi}{r^2}\right\}$$

$$-\left\{k_s F_{55}+\frac{F_{662}}{4}\right\}\left\{r\frac{\partial \phi}{\partial r}+\phi\right\}=0, \tag{13b}$$

$$\left\{F_{33}+\frac{F_{552}}{4}\right\}\left\{\frac{\partial^2 \phi}{\partial r^2}+\frac{1}{r}\frac{\partial \phi}{\partial r}-\frac{\phi}{r^2}\right\}+\left\{F_{22}-F_{33}+\frac{F_{572}}{2}-\frac{F_{552}}{4}\right\}\left\{\frac{\partial^3 w}{\partial r^3}+\frac{1}{r}\frac{\partial^2 w}{\partial r^2}-\frac{1}{r^2}\frac{\partial w}{\partial r}\right\}$$

$$+\left\{k_s F_{55}+\frac{F_{662}}{4}\right\}\left\{\frac{\partial w}{\partial r}-\phi\right\}-F_{11}\left\{\frac{\partial^2 u}{\partial r^2}+\frac{1}{r}\frac{\partial u}{r}-\frac{u}{r^2}\right\}=0. \tag{13c}$$

And, boundary conditions at $r=R_i$ and R_o read

$$\delta u=0, \quad \text{or} \quad \left(F_{11}-B_{11}\right)r\frac{\partial^2 w}{\partial r^2}+\left(F_{11}^*-B_{11}^*\right)\frac{\partial w}{\partial r}+A_{11}r\frac{\partial u}{\partial r}+A_{11}^* u-F_{11}r\frac{\partial \phi}{\partial r}-F_{11}^*\phi-rN^T=0, \tag{14a}$$

$$\delta w=0, \quad \text{or} \quad \left\{2F_{22}-D_{11}-F_{33}-A_{552}+F_{572}-\frac{F_{552}}{4}\right\}\left\{\frac{\partial^3 w}{\partial r^3}+\frac{1}{r}\frac{\partial^2 w}{\partial r^2}-\frac{1}{r^2}\frac{\partial w}{\partial r}\right\}$$

$$+\left\{\frac{F_{662}}{4}+k_s F_{55}\right\}\frac{\partial w}{\partial r}+\left(B_{11}-F_{11}\right)\left\{\frac{\partial^2 u}{\partial r^2}+\frac{1}{r}\frac{\partial u}{\partial r}-\frac{u}{r^2}\right\}$$

$$+\left\{F_{33}-F_{22}-\frac{F_{572}}{2}+\frac{F_{552}}{4}\right\}\left\{\frac{\partial^2 \phi}{\partial r^2}+\frac{1}{r}\frac{\partial \phi}{\partial r}-\frac{\phi}{r^2}\right\}-\left\{\frac{F_{662}}{4}+k_s F_{55}\right\}\phi=0, \tag{14b}$$

$$\delta\left(\frac{\partial w}{\partial r}\right)=0, \qquad \text{or} \qquad \left\{D_{11}-2F_{22}+F_{33}+A_{552}-F_{572}+\frac{F_{552}}{4}\right\}r\frac{\partial^2 w}{\partial r^2}$$

$$+\left\{D_{11}^{*}-2F_{22}^{*}+F_{33}^{*}-A_{552}+F_{572}-\frac{F_{552}}{4}\right\}\frac{\partial w}{\partial r}$$

$$+\left(F_{11}-B_{11}\right)r\frac{\partial u}{\partial r}+\left(F_{11}^{*}-B_{11}^{*}\right)u+\left\{F_{22}-F_{33}+\frac{F_{572}}{2}-\frac{F_{552}}{4}\right\}r\frac{\partial \phi}{\partial r}$$

$$+\left\{F_{22}^{*}-F_{33}^{*}-\frac{F_{572}}{2}+\frac{F_{552}}{4}\right\}\phi+r\left(M^{T}-N_{f}^{T}\right)=0, \tag{14c}$$

$$\delta\phi=0, \qquad \text{or} \qquad \left\{F_{22}-F_{33}+\frac{F_{572}}{2}-\frac{F_{552}}{4}\right\}r\frac{\partial^2 w}{\partial r^2}+\left\{F_{22}^{*}-F_{33}^{*}-\frac{F_{572}}{2}+\frac{F_{552}}{4}\right\}\frac{\partial w}{\partial r}$$

$$-F_{11}r\frac{\partial u}{\partial r}-F_{11}^{*}u+\left\{F_{33}+\frac{F_{552}}{4}\right\}r\frac{\partial \phi}{\partial r}+\left\{F_{33}^{*}-\frac{F_{552}}{4}\right\}\phi+rN_{f}^{T}=0. \tag{14d}$$

Coefficients and thermal loading terms in Eqs. (13) and (14) are found to be,

$$\left\{A_{11},B_{11},D_{11},F_{11},F_{22},F_{33}\right\}=\int_{-h/2}^{h/2}\frac{E(z)}{1-\nu^2(z)}\left\{1,z,z^2,f,zf,f^2\right\}dz, \tag{15a}$$

$$\left\{A_{552},F_{552},F_{572},F_{662}\right\}=\int_{-h/2}^{h/2}\frac{E(z)l^2(z)}{2(1+\nu(z))}\left\{1,f'^2,f',f''^2\right\}dz, \tag{15b}$$

$$F_{55}=\int_{-h/2}^{h/2}\frac{E(z)}{2(1+\nu(z))}f'^2dz, \tag{15c}$$

$$\left\{A_{11}^{*},B_{11}^{*},D_{11}^{*},F_{11}^{*},F_{22}^{*},F_{33}^{*}\right\}=\int_{-h/2}^{h/2}\frac{E(z)\nu(z)}{1-\nu^2(z)}\left\{1,z,z^2,f,zf,f^2\right\}dz, \tag{15d}$$

$$\left\{N^{T},M^{T},N_{f}^{T}\right\}=\int_{-h/2}^{h/2}\frac{E(z)\alpha(z)\theta(z)}{1-\nu(z)}\left\{1,z,f\right\}dz. \tag{15e}$$

k_s in Eqs. (13b) and (14b) is the shear correction factor, which assumes a value of unity in third-order shear deformation theory and $\pi^2/12$ in Mindlin plate theory. A shear correction factor is not included in the formulation based on Kirchhoff plate theory. Thermally induced force and moment given in Eq. (15e) appear in the boundary conditions (14a), (14c), and (14d). Note that governing equations conveyed by Eq. (13) are applicable for both annular and circular micro-plates. But, boundary condition specifications are dependent upon the plate type as will be delineated in Section 3.

2.2. Formulation for free vibrations

In this section, we consider free vibrations of a graded annular or circular micro-plate, that is subjected to an initial thermal stress field. Micro-plate geometry is given in Fig. 1. For the free vibrations problem, Hamilton's principle is expressed as

$$\delta\int_{t_1}^{t_2}(K-U)dt=0, \tag{16}$$

where K is kinetic energy, and U is strain energy. U is a sum of two energy terms in the form [31,32]

$$U=U_S+U_T. \tag{17}$$

U_S is the strain energy corresponding to deformation field and U_T is due to initial thermal stresses. The expressions of $K, U_S,$ and U_T are as follows:

$$K = \frac{1}{2}\int_{-h/2}^{h/2}\int_{R_i}^{R_o} \rho(z)\left(\dot{u}_r^2 + \dot{u}_z^2\right) 2\pi r dr, \tag{18a}$$

$$U_S = \frac{1}{2}\int_{-h/2}^{h/2}\int_{R_i}^{R_o} \left\{\left(\sigma_{rr} + \sigma_{rr}^T\right)\varepsilon_{rr} + \left(\sigma_{\theta\theta} + \sigma_{\theta\theta}^T\right)\varepsilon_{\theta\theta} + 2\left(\sigma_{rz}\varepsilon_{rz} + m_{r\theta}\chi_{r\theta} + m_{z\theta}\chi_{z\theta}\right)\right\} 2\pi r dr dz, \tag{18b}$$

$$U_T = -\frac{1}{2}\int_{-h/2}^{h/2}\int_{R_i}^{R_o} \sigma_{rr}^T \left(\frac{dw}{dr}\right)^2 2\pi r dr. \tag{18c}$$

σ_{rr}^T and $\sigma_{\theta\theta}^T$ are defined by

$$\sigma_{rr}^T = \sigma_{\theta\theta}^T = \frac{E(z)\alpha(z)\theta(z)}{1-\nu(z)}. \tag{19}$$

Applying Hamilton's principle, we derive the governing partial differential equations as given below

$$\left(F_{11} - B_{11}\right)\left\{\frac{\partial^3 w}{\partial r^3} + \frac{1}{r}\frac{\partial^2 w}{\partial r^2} - \frac{1}{r^2}\frac{\partial w}{\partial r}\right\} + A_{11}\left\{\frac{\partial^2 u}{\partial r^2} + \frac{1}{r}\frac{\partial u}{\partial r} - \frac{u}{r^2}\right\} - F_{11}\left\{\frac{\partial^2 \phi}{\partial r^2} + \frac{1}{r}\frac{\partial \phi}{\partial r} - \frac{\phi}{r^2}\right\}$$

$$= I_1\frac{\partial^2 u}{\partial t^2} + \left(I_4 - I_2\right)\frac{\partial^3 w}{\partial r \partial t^2} - I_4\frac{\partial^2 \phi}{\partial t^2}, \tag{20a}$$

$$\left\{2F_{22} - D_{11} - F_{33} - A_{552} + F_{572} - \frac{F_{552}}{4}\right\}\left\{r\frac{\partial^4 w}{\partial r^4} + 2\frac{\partial^3 w}{\partial r^3} - \frac{1}{r}\frac{\partial^2 w}{\partial r^2} + \frac{1}{r^2}\frac{\partial w}{\partial r}\right\}$$

$$+\left\{\frac{F_{662}}{4} + k_s F_{55} - N^T\right\}\left\{r\frac{\partial^2 w}{\partial r^2} + \frac{\partial w}{\partial r}\right\} + \left(B_{11} - F_{11}\right)\left\{r\frac{\partial^3 u}{\partial r^3} + 2\frac{\partial^2 u}{\partial r^2} - \frac{1}{r}\frac{\partial u}{\partial r} + \frac{u}{r^2}\right\}$$

$$+\left\{F_{33} - F_{22} - \frac{F_{572}}{2} + \frac{F_{552}}{4}\right\}\left\{r\frac{\partial^3 \phi}{\partial r^3} + 2\frac{\partial^2 \phi}{\partial r^2} - \frac{1}{r}\frac{\partial \phi}{\partial r} + \frac{\phi}{r^2}\right\} - \left\{k_s F_{55} + \frac{F_{662}}{4}\right\}\left\{r\frac{\partial \phi}{\partial r} + \phi\right\}$$

$$= I_1 r\frac{\partial^2 w}{\partial t^2} + (2I_5 - I_3 - I_6)\left\{\frac{\partial^3 w}{\partial r \partial t^2} + r\frac{\partial^4 w}{\partial r^2 \partial t^2}\right\} + (I_2 - I_4)\left\{\frac{\partial^2 u}{\partial t^2} + r\frac{\partial^3 u}{\partial r \partial t^2}\right\}$$

$$+ (I_6 - I_5)\left\{\frac{\partial^2 \phi}{\partial t^2} + r\frac{\partial^3 \phi}{\partial r \partial t^2}\right\}, \tag{20b}$$

$$\left\{F_{33} + \frac{F_{552}}{4}\right\}\left\{\frac{\partial^2 \phi}{\partial r^2} + \frac{1}{r}\frac{\partial \phi}{\partial r} - \frac{\phi}{r^2}\right\} + \left\{F_{22} - F_{33} + \frac{F_{572}}{2} - \frac{F_{552}}{4}\right\}\left\{\frac{\partial^3 w}{\partial r^3} + \frac{1}{r}\frac{\partial^2 w}{\partial r^2} - \frac{1}{r^2}\frac{\partial w}{\partial r}\right\}$$

$$+ \left\{k_s F_{55} + \frac{F_{662}}{4}\right\}\left\{\frac{\partial w}{\partial r} - \phi\right\} - F_{11}\left\{\frac{\partial^2 u}{\partial r^2} + \frac{1}{r}\frac{\partial u}{\partial r} - \frac{u}{r^2}\right\}$$

$$= I_6\frac{\partial^2 \phi}{\partial t^2} + (I_5 - I_6)\frac{\partial^3 w}{\partial r \partial t^2} - I_4\frac{\partial^2 u}{\partial t^2}. \tag{20c}$$

And, boundary conditions at $r = R_i, R_o$ are obtained as

$$\delta u = 0, \text{ or } (F_{11} - B_{11})r\frac{\partial^2 w}{\partial r^2} + \left(F_{11}^* - B_{11}^*\right)\frac{\partial w}{\partial r} + A_{11} r\frac{\partial u}{\partial r} + A_{11}^* u - F_{11} r\frac{\partial \phi}{\partial r} - F_{11}^*\phi = 0, \tag{21a}$$

$$\delta w = 0, \quad \text{or} \quad \left\{2F_{22} - D_{11} - F_{33} - A_{552} + F_{572} - \frac{F_{552}}{4}\right\}\left\{\frac{\partial^3 w}{\partial r^3} + \frac{1}{r}\frac{\partial^2 w}{\partial r^2} - \frac{1}{r^2}\frac{\partial w}{\partial r}\right\}$$

$$+ \left\{\frac{F_{662}}{4} + k_s F_{55} - N^T\right\}\frac{\partial w}{\partial r} + (B_{11} - F_{11})\left\{\frac{\partial^2 u}{\partial r^2} + \frac{1}{r}\frac{\partial u}{\partial r} - \frac{u}{r^2}\right\}$$

$$+ \left\{F_{33} - F_{22} - \frac{F_{572}}{2} + \frac{F_{552}}{4}\right\}\left\{\frac{\partial^2 \phi}{\partial r^2} + \frac{1}{r}\frac{\partial \phi}{\partial r} - \frac{\phi}{r^2}\right\} - \left\{\frac{F_{662}}{4} + k_s F_{55}\right\}\phi$$

$$= (2I_5 - I_3 - I_6)\frac{\partial^3 w}{\partial r \partial t^2} + (I_2 - I_4)\frac{\partial^2 u}{\partial t^2}, \tag{21b}$$

$$\delta\left(\frac{\partial w}{\partial r}\right) = 0, \quad \text{or} \quad \left\{D_{11} - 2F_{22} + F_{33} + A_{552} - F_{572} + \frac{F_{552}}{4}\right\} r\frac{\partial^2 w}{\partial r^2}$$

$$+ \left\{D_{11}^* - 2F_{22}^* + F_{33}^* - A_{552} + F_{572} - \frac{F_{552}}{4}\right\}\frac{\partial w}{\partial r}$$

$$+\left(F_{11}-B_{11}\right)r\frac{\partial u}{\partial r}+\left(F_{11}^{*}-B_{11}^{*}\right)u+\left\{F_{22}-F_{33}+\frac{F_{572}}{2}-\frac{F_{552}}{4}\right\}r\frac{\partial\phi}{\partial r}$$

$$+\left\{F_{22}^{*}-F_{33}^{*}-\frac{F_{572}}{2}+\frac{F_{552}}{4}\right\}\phi=0, \tag{21c}$$

$$\delta\phi=0, \quad \text{or} \quad \left\{F_{22}-F_{33}+\frac{F_{572}}{2}-\frac{F_{552}}{4}\right\}r\frac{\partial^{2}w}{\partial r^{2}}+\left\{F_{22}^{*}-F_{33}^{*}-\frac{F_{572}}{2}+\frac{F_{552}}{4}\right\}\frac{\partial w}{\partial r}$$

$$-F_{11}r\frac{\partial u}{\partial r}-F_{11}^{*}u+\left\{F_{33}+\frac{F_{552}}{4}\right\}r\frac{\partial\phi}{\partial r}+\left\{F_{33}^{*}-\frac{F_{552}}{4}\right\}\phi=0. \tag{21d}$$

Inertia coefficients in Eqs. (20) and (21) are of the forms

$$\left\{I_1,I_2,I_3,I_4,I_5,I_6\right\}=\int_{-h/2}^{h/2}\rho(z)\left\{1,z,z^{2},f,zf,f^{2}\right\}dz. \tag{22}$$

Notice that thermally induced constant force N^{T} enters free vibration formulation through Eqs. (20b) and (21b). Thermally induced moment however does not affect governing equations and boundary conditions because of the assumed form of strain energy due to initial thermal stresses. This form, which is given by Eq. (18c) and proposed by Raju and Gao [33, 34], includes only the resultant thermal force. We also note that the terms $\left(\sigma_{rr}+\sigma_{rr}^{T}\right)$ and $\left(\sigma_{\theta\theta}+\sigma_{\theta\theta}^{T}\right)$ in Eq. (18b), where σ_{rr} and $\sigma_{\theta\theta}$ are given by Eq. (6a), are independent of temperature. Thus, use of Eqs. (18b) and (18c) in Hamilton's principle does not introduce terms involving thermal bending moment in the resulting governing equations and boundary conditions.

3. Numerical solution

Numerical solutions are developed for an annular micro-plate simply supported at $r = R_i, R_o$ as illustrated in Fig. 1 and a simply-supported circular micro-plate. Differential quadrature method is employed in the solution of the partial differential equations and associated boundary conditions. First step in the solution is definition of normalized quantities, which are as follows:

$$\xi = \frac{r - R_i}{R_o - R_i}, \qquad \gamma = \frac{R_i}{R_o - R_i}, \qquad \eta = \frac{R_o - R_i}{h}, \qquad \chi = \xi + \gamma, \tag{23a}$$

$$\tau = \frac{1}{R_o - R_i}\sqrt{\frac{A_{110}}{I_{10}}}t, \tag{23b}$$

$$\{\overline{u}, \overline{w}\} = \frac{\{u, w\}}{h}, \qquad \varphi = \phi, \tag{23c}$$

$$\left\{\overline{A}_{11}, \overline{B}_{11}, \overline{D}_{11}, \overline{F}_{11}, \overline{F}_{22}, \overline{F}_{33}, \overline{F}_{55}\right\} = \left\{\frac{A_{11}}{A_{110}}, \frac{B_{11}}{hA_{110}}, \frac{D_{11}}{h^2A_{110}}, \frac{F_{11}}{hA_{110}}, \frac{F_{22}}{h^2A_{110}}, \frac{F_{33}}{h^2A_{110}}, \frac{F_{55}}{A_{110}}\right\}, \tag{23d}$$

$$\left\{\overline{A}_{552}, \overline{F}_{552}, \overline{F}_{572}, \overline{F}_{662}\right\} = \left\{\frac{A_{552}}{h^2A_{110}}, \frac{F_{552}}{h^2A_{110}}, \frac{F_{572}}{h^2A_{110}}, \frac{F_{662}}{A_{110}}\right\}, \tag{23e}$$

$$\left\{\overline{A}_{11}^*, \overline{B}_{11}^*, \overline{D}_{11}^*, \overline{F}_{11}^*, \overline{F}_{22}^*, \overline{F}_{33}^*\right\} = \left\{\frac{A_{11}^*}{A_{110}}, \frac{B_{11}^*}{hA_{110}}, \frac{D_{11}^*}{h^2A_{110}}, \frac{F_{11}^*}{hA_{110}}, \frac{F_{22}^*}{h^2A_{110}}, \frac{F_{33}^*}{h^2A_{110}}\right\}, \tag{23f}$$

$$\left\{\overline{N}^T, \overline{M}^T, \overline{N}_f^T\right\} = \left\{\frac{N^T}{A_{110}}, \frac{M^T}{hA_{110}}, \frac{N_f^T}{hA_{110}}\right\}, \tag{23g}$$

$$\left\{\bar{I}_1, \bar{I}_2, \bar{I}_3, \bar{I}_4, \bar{I}_5, \bar{I}_6\right\} = \left\{\frac{I_1}{I_{10}}, \frac{I_2}{hI_{10}}, \frac{I_3}{h^2I_{10}}, \frac{I_4}{hI_{10}}, \frac{I_5}{h^2I_{10}}, \frac{I_6}{h^2I_{10}}\right\}. \tag{23h}$$

A_{110} and I_{10} in the above definitions are reference values of A_{11} and I_1 calculated by considering a homogeneous plate, whose properties are equal to those of the functionally graded plate at $z=-h/2$.

In differential quadrature method, an m^{th} order partial derivative is approximated as

$$\left.\frac{\partial^m u(r,t)}{\partial r^m}\right|_{r=r_i} = \sum_{k=1}^{N} C_{ik}^{(m)} u(r_k,t), \qquad i=1,\ldots,N, \tag{24}$$

where N is number of nodes, and $C_{ik}^{(m)}$ are weighting coefficients [35]. Nodal points are enforced to be shifted Chebyshev-Gauss-Lobatto points [36] through the relation

$$r_k = \frac{1}{2}\left\{1-\cos\left(\frac{\pi(k-1)}{N-1}\right)\right\}, \qquad k=1,\ldots,N. \tag{25}$$

3.1. Numerical solution for static bending

By utilizing Eq. (23) and implementing the differential quadrature method, governing partial differential equations for the static bending problem are reduced to series forms, which are given by

$$\frac{1}{\eta}\left(\bar{F}_{11}-\bar{B}_{11}\right)\left\{\sum_{k=1}^{N} C_{ik}^{(3)}\bar{w}_{0k} + \frac{1}{\chi_i}\sum_{k=1}^{N} C_{ik}^{(2)}\bar{w}_{0k} - \frac{1}{\chi_i^2}\sum_{k=1}^{N} C_{ik}^{(1)}\bar{w}_{0k}\right\}$$

$$+\bar{A}_{11}\left\{\sum_{k=1}^{N} C_{ik}^{(2)}\bar{u}_{0k} + \frac{1}{\chi_i}\sum_{k=1}^{N} C_{ik}^{(1)}\bar{u}_{0k} - \frac{\bar{u}_{0i}}{\chi_i^2}\right\} - \bar{F}_{11}\left\{\sum_{k=1}^{N} C_{ik}^{(2)}\varphi_{0k} + \frac{1}{\chi_i}\sum_{k=1}^{N} C_{ik}^{(1)}\varphi_{0k} - \frac{\varphi_{0i}}{\chi_i^2}\right\} = 0, \tag{26a}$$

$$\frac{1}{\eta}\left\{2\bar{F}_{22}-\bar{D}_{11}-\bar{F}_{33}-\bar{A}_{552}+\bar{F}_{572}-\frac{\bar{F}_{552}}{4}\right\}\left\{\chi_i\sum_{k=1}^{N} C_{ik}^{(4)}\bar{w}_{0k} + 2\sum_{k=1}^{N} C_{ik}^{(3)}\bar{w}_{0k} - \frac{1}{\chi_i}\sum_{k=1}^{N} C_{ik}^{(2)}\bar{w}_{0k}\right.$$

$$+\frac{1}{\chi_i^2}\sum_{k=1}^{N}C_{ik}^{(1)}\bar{w}_{0k}\Big\}+\eta\left\{\frac{\bar{F}_{662}}{4}+k_s\bar{F}_{55}\right\}\left\{\chi_i\sum_{k=1}^{N}C_{ik}^{(2)}\bar{w}_{0k}+\sum_{k=1}^{N}C_{ik}^{(1)}\bar{w}_{0k}\right\}$$

$$+\left(\bar{B}_{11}-\bar{F}_{11}\right)\left\{\chi_i\sum_{k=1}^{N}C_{ik}^{(3)}\bar{u}_{0k}+2\sum_{k=1}^{N}C_{ik}^{(2)}\bar{u}_{0k}-\frac{1}{\chi_i}\sum_{k=1}^{N}C_{ik}^{(1)}\bar{u}_{0k}+\frac{\bar{u}_{0i}}{\chi_i^2}\right\}$$

$$+\left\{\bar{F}_{33}-\bar{F}_{22}-\frac{\bar{F}_{572}}{2}+\frac{\bar{F}_{552}}{4}\right\}\left\{\chi_i\sum_{k=1}^{N}C_{ik}^{(3)}\varphi_{0k}+2\sum_{k=1}^{N}C_{ik}^{(2)}\varphi_{0k}-\frac{1}{\chi_i}\sum_{k=1}^{N}C_{ik}^{(1)}\varphi_{0k}+\frac{\varphi_{0i}}{\chi_i^2}\right\}$$

$$-\eta^2\left\{k_s\bar{F}_{55}+\frac{\bar{F}_{662}}{4}\right\}\left\{\chi_i\sum_{k=1}^{N}C_{ik}^{(1)}\varphi_{0k}+\varphi_{0i}\right\}=0, \tag{26b}$$

$$\left\{\bar{F}_{33}+\frac{\bar{F}_{552}}{4}\right\}\left\{\sum_{k=1}^{N}C_{ik}^{(2)}\varphi_{0k}+\frac{1}{\chi_i}\sum_{k=1}^{N}C_{ik}^{(1)}\varphi_{0k}-\frac{\varphi_{0i}}{\chi_i^2}\right\}$$

$$+\frac{1}{\eta}\left\{\bar{F}_{22}-\bar{F}_{33}+\frac{\bar{F}_{572}}{2}-\frac{\bar{F}_{552}}{4}\right\}\left\{\sum_{k=1}^{N}C_{ik}^{(3)}\bar{w}_{0k}+\frac{1}{\chi_i}\sum_{k=1}^{N}C_{ik}^{(2)}\bar{w}_{0k}-\frac{1}{\chi_i^2}\sum_{k=1}^{N}C_{ik}^{(1)}\bar{w}_{0k}\right\}$$

$$+\eta\left\{k_s\bar{F}_{55}+\frac{\bar{F}_{662}}{4}\right\}\left\{\sum_{k=1}^{N}C_{ik}^{(1)}\bar{w}_{0k}-\eta\varphi_{0i}\right\}-\bar{F}_{11}\left\{\sum_{k=1}^{N}C_{ik}^{(2)}\bar{u}_{0k}+\frac{1}{\chi_i}\sum_{k=1}^{N}C_{ik}^{(1)}\bar{u}_{0k}-\frac{\bar{u}_{0i}}{\chi_i^2}\right\}=0. \tag{26c}$$

In all three equations $i=1,\ldots,N$. For a simply supported annular micro-plate as depicted in Fig. 1, boundary conditions at $r=R_i, R_o$ read:

$$\bar{u}_{01}=\bar{u}_{0N}=0, \tag{27a}$$

$$\bar{w}_{01}=\bar{w}_{0N}=0, \tag{27b}$$

$$\left\{\bar{D}_{11}-\bar{F}_{22}+\bar{A}_{552}-\frac{\bar{F}_{572}}{2}\right\}\gamma\sum_{k=1}^{N}C_{1k}^{(2)}\bar{w}_{0k}$$

$$+\left\{\bar{D}_{11}^{*}-\bar{F}_{22}^{*}-\bar{A}_{552}+\frac{\bar{F}_{572}}{2}\right\}\sum_{k=1}^{N}C_{1k}^{(1)}\bar{w}_{0k}-\eta\bar{B}_{11}\gamma\sum_{k=1}^{N}C_{1k}^{(1)}\bar{u}_{0k}$$

$$+\eta\left\{\bar{F}_{22}+\frac{\bar{F}_{572}}{2}\right\}\gamma\sum_{k=1}^{N}C_{1k}^{(1)}\varphi_{0k}+\eta\left\{\bar{F}_{22}^{*}-\frac{\bar{F}_{572}}{2}\right\}\varphi_{01}+\eta^2\gamma\bar{M}^{T}$$

$$=\left\{\bar{D}_{11}-\bar{F}_{22}+\bar{A}_{552}-\frac{\bar{F}_{572}}{2}\right\}(1+\gamma)\sum_{k=1}^{N}C_{Nk}^{(2)}\bar{w}_{0k}$$

$$+\left\{\bar{D}_{11}^{*}-\bar{F}_{22}^{*}-\bar{A}_{552}+\frac{\bar{F}_{572}}{2}\right\}\sum_{k=1}^{N}C_{Nk}^{(1)}\bar{w}_{0k}-\eta\bar{B}_{11}(1+\gamma)\sum_{k=1}^{N}C_{Nk}^{(1)}\bar{u}_{0k}$$

$$+\eta\left\{\bar{F}_{22}+\frac{\bar{F}_{572}}{2}\right\}(1+\gamma)\sum_{k=1}^{N}C_{Nk}^{(1)}\varphi_{0k}+\eta\left\{\bar{F}_{22}^{*}-\frac{\bar{F}_{572}}{2}\right\}\varphi_{0N}+\eta^{2}(1+\gamma)\bar{M}^{T}=0, \tag{27c}$$

$$\left\{\bar{F}_{22}-\bar{F}_{33}+\frac{\bar{F}_{572}}{2}-\frac{\bar{F}_{552}}{4}\right\}\gamma\sum_{k=1}^{N}C_{1k}^{(2)}\bar{w}_{0k}+\left\{\bar{F}_{22}^{*}-\bar{F}_{33}^{*}-\frac{\bar{F}_{572}}{2}+\frac{\bar{F}_{552}}{4}\right\}\sum_{k=1}^{N}C_{1k}^{(1)}\bar{w}_{0k}$$

$$-\eta\bar{F}_{11}\gamma\sum_{k=1}^{N}C_{1k}^{(1)}\bar{u}_{0k}+\eta\left\{\bar{F}_{33}+\frac{\bar{F}_{552}}{4}\right\}\gamma\sum_{k=1}^{N}C_{1k}^{(1)}\varphi_{0k}+\eta\left\{\bar{F}_{33}^{*}-\frac{\bar{F}_{552}}{4}\right\}\varphi_{01}+\eta\gamma\bar{N}_{f}^{T}$$

$$=\left\{\bar{F}_{22}-\bar{F}_{33}+\frac{\bar{F}_{572}}{2}-\frac{\bar{F}_{552}}{4}\right\}(1+\gamma)\sum_{k=1}^{N}C_{Nk}^{(2)}\bar{w}_{0k}+\left\{\bar{F}_{22}^{*}-\bar{F}_{33}^{*}-\frac{\bar{F}_{572}}{2}+\frac{\bar{F}_{552}}{4}\right\}\sum_{k=1}^{N}C_{Nk}^{(1)}\bar{w}_{0k}$$

$$-\eta\bar{F}_{11}(1+\gamma)\sum_{k=1}^{N}C_{Nk}^{(1)}\bar{u}_{0k}+\eta\left\{\bar{F}_{33}+\frac{\bar{F}_{552}}{4}\right\}(1+\gamma)\sum_{k=1}^{N}C_{Nk}^{(1)}\varphi_{0k}+\eta\left\{\bar{F}_{33}^{*}-\frac{\bar{F}_{552}}{4}\right\}\varphi_{0N}+\eta(1+\gamma)\bar{N}_{f}^{T}=0. \tag{27d}$$

In the numerical solution of the circular micro-plate problem, plate profile is assumed to be annular with a very small inner radius R_i. For a circular micro-plate simply-supported around the periphery, the aforementioned equations are applicable at $r=R_o$. Boundary conditions at $r=R_i$ however need to be rearranged as

$$\bar{u}_{01}=0, \tag{28a}$$

$$\left\{2\bar{F}_{22}-\bar{D}_{11}-\bar{F}_{33}-\bar{A}_{552}+\bar{F}_{572}-\frac{\bar{F}_{552}}{4}\right\}\left\{\sum_{k=1}^{N}C_{1k}^{(3)}\bar{w}_{0k}+\frac{1}{\gamma_{\varepsilon}}\sum_{k=1}^{N}C_{1k}^{(2)}\bar{w}_{0k}\right\}$$

$$+\eta\left(\bar{B}_{11}-\bar{F}_{11}\right)\left\{\sum_{k=1}^{N}C_{1k}^{(2)}\bar{u}_{0k}+\frac{1}{\gamma_{\varepsilon}}\sum_{k=1}^{N}C_{1k}^{(1)}\bar{u}_{0k}\right\}$$

$$+\eta\left\{\bar{F}_{33}-\bar{F}_{22}-\frac{\bar{F}_{572}}{2}+\frac{\bar{F}_{552}}{4}\right\}\left\{\sum_{k=1}^{N}C_{1k}^{(2)}\varphi_{0k}+\frac{1}{\gamma_{\varepsilon}}\sum_{k=1}^{N}C_{1k}^{(1)}\varphi_{0k}\right\}=0, \tag{28b}$$

$$\sum_{k=1}^{N}C_{1k}^{(1)}\bar{w}_{0k}=0, \tag{28c}$$

$$\varphi_1=0. \tag{28d}$$

γ_{ε} in Eq. (28b) is a sufficiently small number.

For both annular and circular micro-plate problems, governing equations and boundary conditions are consolidated into a matrix equation of the form

$$\mathbf{K_S X_0}+\mathbf{Q}=\mathbf{0}, \tag{29}$$

where $\mathbf{K_S}$ is stiffness matrix, $\mathbf{Q}$ is generalized distributed thermal load vector, and $\mathbf{X_0}$ is nodal displacement vector, which is expressed as follows:

$$\mathbf{X_0}=\left\{\{\bar{u}_{0i}\}^{\mathrm{T}},\{\bar{w}_{0i}\}^{\mathrm{T}},\{\varphi_{0i}\}^{\mathrm{T}}\right\} \qquad i=1,2,\ldots,N. \tag{30}$$

All required field variables can be determined once the solution of Eq. (29) is obtained.

3.2. Numerical solution for free vibrations

By using the normalizations given by Eq. (23), series forms of the governing equations are derived as presented below:

$$\frac{1}{\eta}\left(\bar{F}_{11}-\bar{B}_{11}\right)\left\{\sum_{k=1}^{N}C_{ik}^{(3)}\bar{w}_k^*+\frac{1}{\chi_i}\sum_{k=1}^{N}C_{ik}^{(2)}\bar{w}_k^*-\frac{1}{\chi_i^2}\sum_{k=1}^{N}C_{ik}^{(1)}\bar{w}_k^*\right\}$$

$$+\bar{A}_{11}\left\{\sum_{k=1}^{N}C_{ik}^{(2)}\bar{u}_k^*+\frac{1}{\chi_i}\sum_{k=1}^{N}C_{ik}^{(1)}\bar{u}_k^*-\frac{\bar{u}_i^*}{\chi_i^2}\right\}-\bar{F}_{11}\left\{\sum_{k=1}^{N}C_{ik}^{(2)}\varphi_k^*+\frac{1}{\chi_i}\sum_{k=1}^{N}C_{ik}^{(1)}\varphi_k^*-\frac{\varphi_i^*}{\chi_i^2}\right\}$$

$$=\bar{I}_1\ddot{\bar{u}}_i^*+\frac{1}{\eta}\left(\bar{I}_4-\bar{I}_2\right)\sum_{k=1}^{N}C_{ik}^{(1)}\ddot{\bar{w}}_k^*-\bar{I}_4\ddot{\varphi}_i^*, \tag{31a}$$

$$\frac{1}{\eta}\left\{2\bar{F}_{22}-\bar{D}_{11}-\bar{F}_{33}-\bar{A}_{552}+\bar{F}_{572}-\frac{\bar{F}_{552}}{4}\right\}\left\{\chi_i\sum_{k=1}^{N}C_{ik}^{(4)}\bar{w}_k^*+2\sum_{k=1}^{N}C_{ik}^{(3)}\bar{w}_k^*-\frac{1}{\chi_i}\sum_{k=1}^{N}C_{ik}^{(2)}\bar{w}_k^*\right.$$

$$\left.+\frac{1}{\chi_i^2}\sum_{k=1}^{N}C_{ik}^{(1)}\bar{w}_k^*\right\}+\eta\left\{\frac{\bar{F}_{662}}{4}+k_s\bar{F}_{55}-\bar{N}^T\right\}\left\{\chi_i\sum_{k=1}^{N}C_{ik}^{(2)}\bar{w}_k^*+\sum_{k=1}^{N}C_{ik}^{(1)}\bar{w}_k^*\right\}$$

$$+\left(\bar{B}_{11}-\bar{F}_{11}\right)\left\{\chi_i\sum_{k=1}^{N}C_{ik}^{(3)}\bar{u}_k^*+2\sum_{k=1}^{N}C_{ik}^{(2)}\bar{u}_k^*-\frac{1}{\chi_i}\sum_{k=1}^{N}C_{ik}^{(1)}\bar{u}_k^*+\frac{\bar{u}_i^*}{\chi_i^2}\right\}$$

$$+\left\{\bar{F}_{33}-\bar{F}_{22}-\frac{\bar{F}_{572}}{2}+\frac{\bar{F}_{552}}{4}\right\}\left\{\chi_i\sum_{k=1}^{N}C_{ik}^{(3)}\varphi_k^*+2\sum_{k=1}^{N}C_{ik}^{(2)}\varphi_k^*-\frac{1}{\chi_i}\sum_{k=1}^{N}C_{ik}^{(1)}\varphi_k^*+\frac{\varphi_i^*}{\chi_i^2}\right\}$$

$$-\eta^2\left\{k_s\bar{F}_{55}+\frac{\bar{F}_{662}}{4}\right\}\left\{\chi_i\sum_{k=1}^{N}C_{ik}^{(1)}\varphi_k^*+\varphi_i^*\right\}$$

$$=\eta\chi_i\bar{I}_1\ddot{\bar{w}}_i^*+\frac{1}{\eta}\left(2\bar{I}_5-\bar{I}_3-\bar{I}_6\right)\left\{\sum_{k=1}^{N}C_{ik}^{(1)}\ddot{\bar{w}}_k^*+\chi_i\sum_{k=1}^{N}C_{ik}^{(2)}\ddot{\bar{w}}_k^*\right\}+\left(\bar{I}_2-\bar{I}_4\right)\left\{\ddot{\bar{u}}_i^*+\chi_i\sum_{k=1}^{N}C_{ik}^{(1)}\ddot{\bar{u}}_k^*\right\}$$

$$+\left(\bar{I}_6-\bar{I}_5\right)\left\{\ddot{\varphi}_i^*+\chi_i\sum_{k=1}^{N}C_{ik}^{(1)}\ddot{\varphi}_k^*\right\}, \tag{31b}$$

$$\left\{\bar{F}_{33}+\frac{\bar{F}_{552}}{4}\right\}\left\{\sum_{k=1}^{N}C_{ik}^{(2)}\varphi_k^*+\frac{1}{\chi_i}\sum_{k=1}^{N}C_{ik}^{(1)}\varphi_k^*-\frac{\varphi_i^*}{\chi_i^2}\right\}$$

$$+\frac{1}{\eta}\left\{\bar{F}_{22}-\bar{F}_{33}+\frac{\bar{F}_{572}}{2}-\frac{\bar{F}_{552}}{4}\right\}\left\{\sum_{k=1}^{N}C_{ik}^{(3)}\bar{w}_k^*+\frac{1}{\chi_i}\sum_{k=1}^{N}C_{ik}^{(2)}\bar{w}_k^*-\frac{1}{\chi_i^2}\sum_{k=1}^{N}C_{ik}^{(1)}\bar{w}_k^*\right\}$$

$$+\eta\left\{k_s\bar{F}_{55}+\frac{\bar{F}_{662}}{4}\right\}\left\{\sum_{k=1}^{N}C_{ik}^{(1)}\bar{w}_k^*-\eta\varphi_i^*\right\}-\bar{F}_{11}\left\{\sum_{k=1}^{N}C_{ik}^{(2)}\bar{u}_k^*+\frac{1}{\chi_i}\sum_{k=1}^{N}C_{ik}^{(1)}\bar{u}_k^*-\frac{\bar{u}_i^*}{\chi_i^2}\right\}$$

$$= \bar{I}_6 \ddot{\varphi}_i^* + \frac{1}{\eta}\left(\bar{I}_5 - \bar{I}_6\right)\sum_{k=1}^{N} C_{ik}^{(1)} \ddot{\bar{w}}_k^* - \bar{I}_4 \ddot{\bar{u}}_i^*. \tag{31c}$$

$i = 1, \ldots, N$ in all three equations. For the simply supported annular micro-plate shown in Fig. 1, boundary conditions at $r = R_i, R_o$ are:

$$\bar{u}_1^* = \bar{u}_N^* = 0, \tag{32a}$$

$$\bar{w}_1^* = \bar{w}_N^* = 0, \tag{32b}$$

$$\left\{\bar{D}_{11} - \bar{F}_{22} + \bar{A}_{552} - \frac{\bar{F}_{572}}{2}\right\}\gamma\sum_{k=1}^{N} C_{1k}^{(2)} \bar{w}_k^* + \left\{\bar{D}_{11}^* - \bar{F}_{22}^* - \bar{A}_{552} + \frac{\bar{F}_{572}}{2}\right\}\sum_{k=1}^{N} C_{1k}^{(1)} \bar{w}_k^* - \eta \bar{B}_{11}\gamma\sum_{k=1}^{N} C_{1k}^{(1)} \bar{u}_k^*$$

$$+ \eta\left\{\bar{F}_{22} + \frac{\bar{F}_{572}}{2}\right\}\gamma\sum_{k=1}^{N} C_{1k}^{(1)} \varphi_k^* + \eta\left\{\bar{F}_{22}^* - \frac{\bar{F}_{572}}{2}\right\}\varphi_1^*$$

$$= \left\{\bar{D}_{11} - \bar{F}_{22} + \bar{A}_{552} - \frac{\bar{F}_{572}}{2}\right\}(1+\gamma)\sum_{k=1}^{N} C_{Nk}^{(2)} \bar{w}_k^*$$

$$+ \left\{\bar{D}_{11}^* - \bar{F}_{22}^* - \bar{A}_{552} + \frac{\bar{F}_{572}}{2}\right\}\sum_{k=1}^{N} C_{Nk}^{(1)} \bar{w}_k^* - \eta \bar{B}_{11}(1+\gamma)\sum_{k=1}^{N} C_{Nk}^{(1)} \bar{u}_k^*$$

$$+ \eta\left\{\bar{F}_{22} + \frac{\bar{F}_{572}}{2}\right\}(1+\gamma)\sum_{k=1}^{N} C_{Nk}^{(1)} \varphi_k^* + \eta\left\{\bar{F}_{22}^* - \frac{\bar{F}_{572}}{2}\right\}\varphi_N^* = 0, \tag{32c}$$

$$\left\{\bar{F}_{22} - \bar{F}_{33} + \frac{\bar{F}_{572}}{2} - \frac{\bar{F}_{552}}{4}\right\}\gamma\sum_{k=1}^{N} C_{1k}^{(2)} \bar{w}_k^* + \left\{\bar{F}_{22}^* - \bar{F}_{33}^* - \frac{\bar{F}_{572}}{2} + \frac{\bar{F}_{552}}{4}\right\}\sum_{k=1}^{N} C_{1k}^{(1)} \bar{w}_k^*$$

$$- \eta \bar{F}_{11}\gamma\sum_{k=1}^{N} C_{1k}^{(1)} \bar{u}_k^* + \eta\left\{\bar{F}_{33} + \frac{\bar{F}_{552}}{4}\right\}\gamma\sum_{k=1}^{N} C_{1k}^{(1)} \varphi_k^* + \eta\left\{\bar{F}_{33}^* - \frac{\bar{F}_{552}}{4}\right\}\varphi_1^*$$

$$= \left\{\bar{F}_{22} - \bar{F}_{33} + \frac{\bar{F}_{572}}{2} - \frac{\bar{F}_{552}}{4}\right\}(1+\gamma)\sum_{k=1}^{N} C_{Nk}^{(2)} \bar{w}_k^* + \left\{\bar{F}_{22}^* - \bar{F}_{33}^* - \frac{\bar{F}_{572}}{2} + \frac{\bar{F}_{552}}{4}\right\}\sum_{k=1}^{N} C_{Nk}^{(1)} \bar{w}_k^*$$

$$- \eta \bar{F}_{11}(1+\gamma)\sum_{k=1}^{N} C_{Nk}^{(1)} \bar{u}_k^* + \eta\left\{\bar{F}_{33} + \frac{\bar{F}_{552}}{4}\right\}(1+\gamma)\sum_{k=1}^{N} C_{Nk}^{(1)} \varphi_k^* + \eta\left\{\bar{F}_{33}^* - \frac{\bar{F}_{552}}{4}\right\}\varphi_N^* = 0. \tag{32d}$$

In the case of the circular micro-plate, these conditions are applicable at $r = R_o$. At $r = R_i$ on the other hand, following equations need to be implemented:

$$\bar{u}_1^* = 0, \tag{33a}$$

$$\left\{2\bar{F}_{22} - \bar{D}_{11} - \bar{F}_{33} - \bar{A}_{552} + \bar{F}_{572} - \frac{\bar{F}_{552}}{4}\right\}\left\{\sum_{k=1}^{N} C_{1k}^{(3)} \bar{w}_k^* + \frac{1}{\gamma_\varepsilon}\sum_{k=1}^{N} C_{1k}^{(2)} \bar{w}_k^*\right\}$$

$$+\eta\left(\bar{B}_{11} - \bar{F}_{11}\right)\left\{\sum_{k=1}^{N} C_{1k}^{(2)} \bar{u}_k^* + \frac{1}{\gamma_\varepsilon}\sum_{k=1}^{N} C_{1k}^{(1)} \bar{u}_k^*\right\}$$

$$+\eta\left\{\bar{F}_{33} - \bar{F}_{22} - \frac{\bar{F}_{572}}{2} + \frac{\bar{F}_{552}}{4}\right\}\left\{\sum_{k=1}^{N} C_{1k}^{(2)} \varphi_k^* + \frac{1}{\gamma_\varepsilon}\sum_{k=1}^{N} C_{1k}^{(1)} \varphi_k^*\right\} = 0, \tag{33b}$$

$$\sum_{k=1}^{N} C_{1k}^{(1)} \bar{w}_k^* = 0, \tag{33c}$$

$$\varphi_1^* = 0. \tag{33d}$$

For both of the annular and circular micro-plate problems, governing equations and boundary conditions are combined and recast into the general form:

$$\mathbf{K_D X}^* + \mathbf{M}\ddot{\mathbf{X}}^* = \mathbf{0}, \tag{34}$$

in which $\mathbf{K_D}$ is the stiffness matrix including initial thermal stresses, and $\mathbf{M}$ is mass matrix. Dynamic displacement vector is expressed as follows:

$$\mathbf{X}^* = \left\{\left\{\bar{u}_i^*\right\}^{\mathrm{T}}, \left\{\bar{w}_i^*\right\}^{\mathrm{T}}, \left\{\varphi_i^*\right\}^{\mathrm{T}}\right\}^{\mathrm{T}}, \qquad i = 1, 2, \ldots, N. \tag{35}$$

By assuming

$$\mathbf{X}^* = \hat{\mathbf{X}}^* \mathrm{e}^{i\omega\tau}, \tag{36}$$

Eq. (34) is reduced to the linear homogeneous system

$$\left(\mathbf{K_D} - \omega^2 \mathbf{M}\right)\hat{\mathbf{X}}^* = \mathbf{0}, \tag{37}$$

where $\hat{\mathbf{X}}^*$ is mode shape vector and ω stands for dimensionless vibration frequency. $\hat{\mathbf{X}}^*$ and ω are given by

$$\hat{\mathbf{X}}^* = \left\{\left\{\hat{\overline{u}}_i^*\right\}^{\mathrm{T}}, \left\{\hat{\overline{w}}_i^*\right\}^{\mathrm{T}}, \left\{\hat{\varphi}_i^*\right\}^{\mathrm{T}}\right\}^{\mathrm{T}}, \tag{38a}$$

$$\omega = \sqrt{\frac{I_{10}}{A_{110}}}\left(R_o - R_i\right)\Omega. \tag{38b}$$

Ω here is the frequency of free vibrations. The deformation mode that a computed frequency represents is identified in the numerical solution by examining the mode shape vector.

4. Numerical results

The particular ceramic and metallic constituents considered are silicon carbide (SiC) and aluminum (Al), whose properties are given by

$$E_c = 427\,\mathrm{GPa}, \quad \nu_c = 0.17, \quad \rho_c = 3100\,\mathrm{kg/m^3}, \quad k_c = 65\,\mathrm{W/(m\cdot K)}, \quad \alpha_c = 4.3(10)^{-6}\,1/\mathrm{K}, \tag{39a}$$

$$E_m = 70\,\mathrm{GPa}, \quad \nu_m = 0.3, \quad \rho_m = 2702\,\mathrm{kg/m^3}, \quad k_m = 204\,\mathrm{W/(m\cdot K)}, \quad \alpha_m = 23.0(10)^{-6}\,1/\mathrm{K}. \tag{39b}$$

For a given material, the value of the length scale parameter can be determined experimentally. This requires development of a modified couple stress theory based solution considering a simple problem such as bending or torsion. Length scale parameter can then be measured by matching the theoretical results to those obtained from experiments. By adopting such a technique, the length scale parameter for epoxy is determined as 17.6 μm [22,37]. However, due to lack of experimental data for length scale parameters of SiC and Al, in the present study we use approximate values. Length scale parameter of the metallic phase is specified as $l_m = 15\,\mu$m, which is a reference value suggested in the literature [20,38]. l_c is taken as 22.5 μm in a number of parametric analyses. In the other cases, it is varied to be able to examine the influence of the length scale parameter variation.

In order to verify the solution methodologies developed, we first present comparisons to the results available in the literature. Fig. 2 shows results pertaining to static bending of a simply-supported annular homogeneous macro-scale plate under the influence of thermal loading. Plate material is silicon carbide, and Kirchhoff plate theory is employed in the computations. l_c and l_m are taken as zero to be able to generate results for the macro-scale annular plate. The figure illustrates that static deformation profile we compute is in perfect agreement with that found by Noda et al. [39]. The second set of comparisons comprises natural frequencies of a freely vibrating simply-supported aluminum circular macro-scale plate subjected to initial thermal stresses. First dimensionless natural frequencies of the homogeneous plate are given in Table 1 for four different loading conditions. Kirchhoff plate theory is used in these parametric analyses. Our findings are in excellent agreement with those given by Raju et al. [34]. Hence, we conclude that proposed techniques lead to numerical results to within a high degree of accuracy.

Numerical results on static bending of FGM micro-plates under thermal loading are provided in Figs. 3-8. In Fig. 3, we present deflections of an annular FGM micro-plate

computed utilizing Kirchhoff, Mindlin and third-order shear deformation theories. The theories are seen to lead to almost identical deformation profiles. Thus, in the computation of the results given in Figs. 4-8, we employed third-order shear deformation theory. Fig. 4 depicts deflections of an annular FGM micro-plate generated by considering three different thermal loading conditions. When the temperature of the upper surface is greater than or equal to that of the lower surface, the micro-plate becomes concave downward. In the case of a lower upper surface, temperature concavity is reversed.

The results provided in Figs. 5 and 6 demonstrate the impact of the length scale parameter ratio l_c/l_m upon static deformation profiles of functionally graded annular and circular micro-plates, respectively. Referring to Eq. (3b), it can be deduced that when $l_c = l_m$, length scale parameter l is constant within the plate. But, if $l_c \neq l_m$, l is a function of the spatial coordinate z; and the ratio l_c/l_m quantifies the degree of length scale parameter variation. From Fig. 5 it is seen that, for a thermally loaded annular micro-plate, static deflection decreases significantly as l_c/l_m increases. This implies that the micro-plate displays a stiffer behavior when the length scale parameter ratio is larger. However, as Fig. 6 indicates, a thermally loaded circular micro-plate is not sensitive to the variations in l_c/l_m. Figs. 7 and 8 show distributions of normalized circumferential and radial stresses in a simply supported annular FGM micro-plate. Both of the stress components are compressive under the given thermal loading condition. Largest magnitudes are computed near the upper surface. These magnitudes are greater for micro-plates displaying a stiffer behavior, i.e., for those possessing larger l_c/l_m values. The influence of the length scale parameter ratio on the radial stress component is in general more pronounced compared to its effect on circumferential stress.

Outcomes of parametric analyses regarding free vibrations under initial thermal stresses are presented in Tables 2 and 3; and Figs. 9-13. All of these results are produced by using third order shear deformation theory. Table 2 tabulates first three dimensionless natural frequencies of a simply supported annular FGM micro-plate. The frequencies correspond to the transverse deformation mode. The findings indicate that each natural frequency is an increasing function of the length scale parameter ratio l_c/l_m, and a decreasing function of the inhomogeneity parameter λ. The rise in l_c/l_m again causes a stiffer response demonstrated by the corresponding rise in the natural frequency. This behavior is consistent with our findings pertaining to static analysis. Similar trends are found to be valid for a simply supported circular FGM micro-plate as indicated by Table 3.

In Figs. 9 and 10, we provide first dimensionless natural frequency ω_1 as a function of boundary temperature difference for simply-supported annular and circular micro-plates, respectively. In each case, ω_1 curve is plotted for four different values of the ratio h/l_m. Note that temperature differences of lower and upper plate surfaces are assumed to be equal, i.e. $\theta_L = \theta_U$. Results given in Fig. 9 reveal that first natural frequency of a simply-supported annular micro-plate is not that sensitive to the variation in temperature difference. However, ω_1 of a circular micro-plate drops significantly as temperature difference increases, as can be seen from Fig. 10. The ratio h/l_m is representative of the degree of size effect. Size dependence is more prevalent when this ratio is relatively small. For both annular and circular micro-plates, first dimensionless frequency increases notably as h/l_m decreases from 4 to 1. This finding is in complete agreement with the physics of the problem since as the component size approaches the realm of micro-scale, size effect causes it to behave in a stiffer manner and leads to significantly smaller deflections and larger natural frequencies.

The effect of h/l_m over a wider domain for a simply-supported annular micro-plate is depicted in Fig. 11. The variation is plotted for four different values of the inhomogeneity parameter λ. ω_1 rises sharply as the ratio h/l_m tends to zero, which is indicative of the size effect. Inhomogeneity parameter is also influential and an increase in its value causes a drop in the dimensionless first natural frequency. From Eq. (2), it follows that, annular and circular micro-plates are both ceramic-rich when $\lambda < 1;$ and metal-rich when $\lambda > 1.$ Thus, ceramic-rich micro-plates display a stiffer vibration behavior compared to metal-rich micro-plates.

Finally, in Figs. 12 and 13, ω_1 is given as functions of h/l_m and the length scale parameter ratio l_c/l_m. The results provided in Fig. 12 for an annular plate and those presented in Fig. 13 for a circular one are in general similar. In both cases, as l_c/l_m is increased from $1/3$ to 2, dimensionless first natural frequency becomes larger. As is the case for static loading, the increase in the length scale parameter ratio causes the micro-plates to display a stiffer behavior.

5. Concluding remarks

We presented new techniques that facilitate solution of static bending and free vibrations problems involving thermally loaded functionally graded annular and circular micro-plates. Governing partial differential equations and corresponding boundary conditions are derived by applying Hamilton's principle in conjunction with modified couple stress theory. Posed problems are then solved numerically utilizing the differential quadrature method, which converts partial derivatives into finite sums in terms of weighting coefficients and functional values. Comparisons to the results provided by Noda et al. [39] and Raju and Gao [34] do verify the proposed thermal analysis procedures. Extensive parametric analyses are conducted

to be able to assess the influences of factors such as applied thermal loading, length scale parameter ratio, problem geometry, and material inhomogeneity.

Our findings illustrate that both type and magnitude of thermal loading have a substantive effect on the mechanical response of graded annular and circular micro-plates. A graded micro-plate under static loading bends concave downwards when the temperature of the upper surface is greater than or equal to that of the lower surface. On the other hand, for freely vibrating annular and circular micro-plates that are under the influence of initial thermal stresses, increase in the body temperature leads to drops in the first dimensionless natural frequency.

Each of the material and geometric parameters l_c/l_m, h/l_m, and λ possesses a strong bearing on the behavior of annular and circular micro-plates. The ratio h/l_m quantifies the extent of size effect since when it is around or smaller than unity, size effect is expected to be noticeable. Our results demonstrate a sharp rise in natural frequency with a drop in h/l_m which is indicative of stiffening at the micro-scale. Such a strengthening in mechanical response is also observed for larger l_c/l_m values and for ceramic-rich plates, for which λ assumes values less than unity.

Annular and circular micro-plates are fabricated for a wide variety of micro-electro-mechanical-systems including acoustic energy harvesters, micro-scale resonators, optical and pressure sensors, and stiction valves. The methods presented could prove useful in accounting for temperature related effects and material inhomogeneity in design studies involving such components. Proposed framework is open to further extension especially through incorporation of large deformations by means of a suitable nonlinear plate theory.

Acknowledgements

Serkan Dag acknowledges the support of the Scientific and Technological Research Council of Turkey (TÜBİTAK) through grant 213M606.

References

[1] Nath S, Manna I, Majumdar JD. Nanomechanical behavior of yttria stabilized zirconia (YSZ) based thermal barrier coating. Ceram Int 2015;41:5247–56.

[2] Singh RK, Zhou Z, Li LKY, Munroe P, Hoffman M, Xie Z. Design of functionally graded carbon coatings against contact damage. Thin Solid Films 2010;518:5769–76.

[3] Ma R, Fang L, Luo Z, Weng L, Song S, Zheng R, Sun H, Fu H. Mechanical performance and in vivo bioactivity of functionally graded PEEK-HA biocomposite materials. J Sol-Gel Sci Techn 2014;70:339–45.

[4] Mehrali M, Shirazi FS, Mehrali M, Metselaar HSC, Kadri NAB, Osman NAA. Dental implants from functionally graded materials. J Biomed Mater Res Part A 2013;101A:3046–57.

[5] Woolley RJ, Skinner SJ. Functionally graded composite $La_2NiO_{4+\delta}$ and $La_4Ni_3O_{10-\delta}$ solid oxide fuel cell cathodes. Solid State Ionics 2014;255:1–5.

[6] Fu Y, Du H, Zhang S. Functionally graded TiN/TiNi shape memory alloy films. Mater Lett 2003;57:2995–9.

[7] Witvrouw A, Mehta A. The use of functionally graded Poly-SiGe layers for MEMS applications. Mater Sci Forum 2005;492–3:255–60.

[8] Hassanin H, Jiang K. Net shape manufacturing of ceramic micro parts with tailored graded layers. J Micromech Microeng 2014;24. Article No: 015018.

[9] Li P, Fang Y, Hu R. Thermoelastic damping in rectangular and circular microplate resonators. J Sound Vib 2012;331:721–733.

[10] Pattnaik PK, Vijayaaditya BH, Srinivas T, Selvarajan A. Optical MEMS pressure sensor using ring resonator on a circular diaphragm. In: Proceedings of the 2005 International Conference on MEMS. Banff, Alberta, Canada; July, 2005.

[11] Olfatnia M, Xu T, Miao JM, Ong LS, Jing XM, Norford L. Piezoelectric circular microdiaphragm based pressure sensors. Sens Actuat A-Phys 2010;163:32–6.

[12] Gietzelt T, Jacobi O, Piotter V, Ruprecht R, Hausselt J. Development of a micro annular gear pump by micro powder injection molding. J Mater Sci 2004;39:2113–9.

[13] Yang F, Chong ACM, Lam DCC, Tong P. Couple stress based strain gradient theory for elasticity. Int J Solids Struct 2002;39:2731–43.

[14] Wang YG, Lin WH, Zhou CL. Nonlinear bending of size-dependent circular microplates based on the modified couple stress theory. Arch Appl Mech 2014;84:391–400.

[15] Zhou SS, Gao XL. A nonclassical model for circular Mindlin plates based on a modified couple stress theory. J Appl Mech-T ASME 2014;81: Paper No: 051014-1.

[16] Wang YG, Lin WH, Liu N. Large amplitude free vibration of size-dependent circular microplates based on the modified couple stress theory. Int J Mech Sci 2013;71:51–7.

[17] Eshraghi I, Dag S, Soltani N. Consideration of spatial variation of the length scale parameter in static and dynamic analyses of functionally graded annular and circular micro-plates. Compos Part B-Eng 2015;78:338–48.

[18] Ansari R, Gholami R, Faghih Shojaei M, Mohammadi V, Sahmani S. Bending, buckling and free vibration analysis of size-dependent functionally graded circular/annular microplates based on the modified strain gradient elasticity theory. Eur J Mech A-Solid 2015;49:251–267.

[19] Reddy JN, Berry J. Nonlinear theories of axisymmetric bending of functionally graded circular plates with modified couple stress. Compos Struct 2012;94:3664–8.

[20] Ke LL, Yang J, Kitipornchai S, Bradford MA, Wang YS. Axisymmetric nonlinear free vibration of size-dependent functionally graded annular microplates. Compos Part B-Eng 2013;53:207–17.

[21] Ke LL, Yang J, Kitipornchai S, Wang YS. Axisymmetric postbuckling analysis of size-dependent functionally graded annular microplates using the physical neutral plane. Int J Eng Sci 2014;81:66–81.

[22] Lam DCC, Yang F, Chong ACM, Wang J, Tong P. Experiments and theory in strain gradient elasticity. J Mech Phys Solids 2003;51:1477–508.

[23] Mori T, Tanaka K. Average stress in matrix and average elastic energy of materials with misfitting inclusions. Acta Metall 1973;21:571–4.

[24] Çömez I. Contact problem of a functionally graded layer resting on a Winkler foundation. Acta Mech 2013;224:2833–43.

[25] Mao JJ, Ke LL, Wang YS. Thermoelastic instability of a functionally graded layer interacting with a homogeneous layer. Int J Mech Sci 2013;99:218–27.

[26] Ohmichi M, Noda N. Conditions of single-valuedness of rotation and displacements for non-homogeneous materials in plane thermoelasticity. J Therm Stresses 2015;38:610–29.

[27] Fallah F, Vahidipoor MK, Nosier A. Post-buckling behavior of functionally graded circular plates under asymmetric transverse and in-plane loadings. Compos Struct 2015;125:477–88.

[28] Su Z, Jin G, Ye T. Three-dimensional vibration analysis of thick functionally graded conical, cylindrical shell and annular plate structures with arbitrary elastic restraints. Compos Struct 2014;118:432–47.

[29] Xin L, Dui G, Yang S, Zhang J. An elasticity solution for functionally graded thick-walled tube subjected to internal pressure. Int J Mech Sci 2014;89:344–9.

[30] Dehrouyeh-Semnani AM, Dehrouyeh M, Torabi-Kafshgari M, Nikkhah-Bahrami M. An investigation into size-dependent vibration damping characteristics of functionally graded viscoelastically damped sandwich microbeams. Int J Eng Sci 2015;96:68–85.

[31] Shi P, Dong CY. Vibration analysis of functionally graded annular plates with mixed boundary conditions in thermal environment. J Sound Vib 2012;331:3649–62.

[32] Nateghi A, Salamat-talab M. Thermal effect on size dependent behavior of functionally graded microbeams based on modified couple stress theory. Compos Struct 2013;96:97–110.

[33] Raju KK, Rao KS. Effect of temperature on the large amplitude vibrations of circular plates. J Sound Vib 1977;54:149–52.

[34] Raju KK, Rao GV. Effect of initial thermal stresses on the large amplitude vibrations of circular plates. J Sound Vib 1978;59:150–2.

[35] Shu C. Differential quadrature and its applications in engineering. Springer-Verlag; 2000.

[36] Ng CHW, Zhao YB, Xiang Y, Wei GW. On the accuracy and stability of a variety of differential quadrature formulations for the vibration analysis of beams. Int J Eng Appl Sci 2009;1:85–101.

[37] Ansari R, Gholami R, Sahmani S. Free vibration analysis of size-dependent functionally graded microbeams based on the strain gradient Timoshenko beam theory. Compos Struct 2011;94:221–8.

[38] Ke LL, Wang YS. Size effect on dynamic stability of functionally graded microbeams based on a modified couple stress theory. Compos Struct 2011;93:342–50.

[39] Noda N, Hetnarski RB, Tanigawa Y. Thermal stresses. Taylor & Francis; 2003.

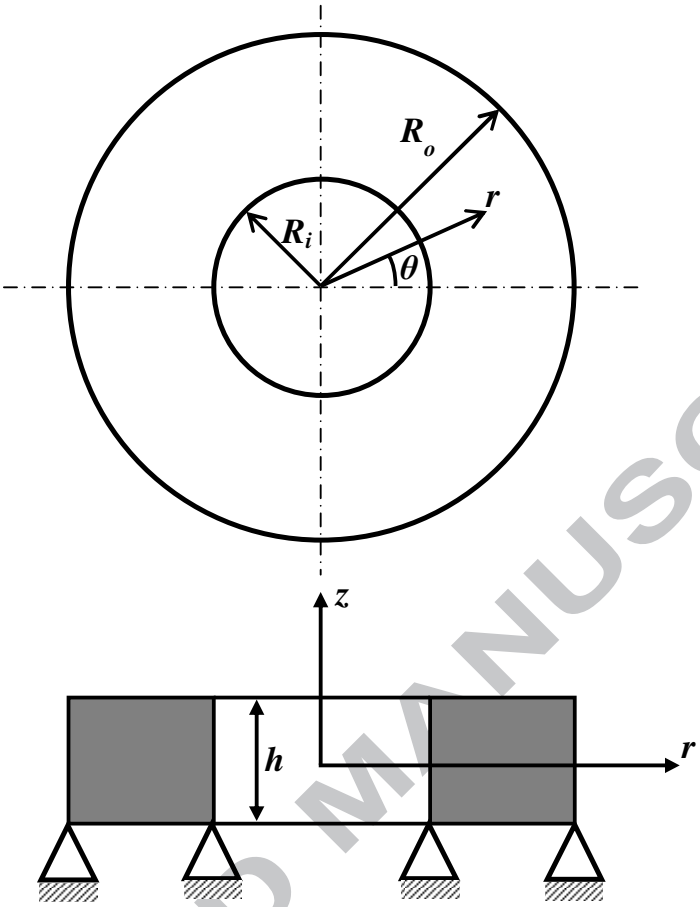

Fig. 1 A functionally graded simply-supported annular micro-plate.

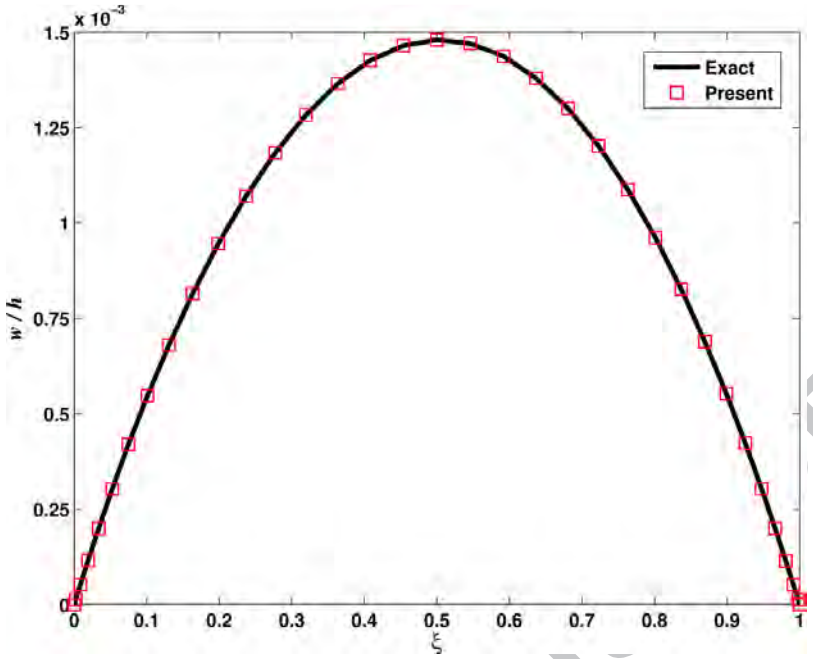

Fig. 2 Static bending deformation of a simply-supported annular silicon carbide plate.

$R_o/h = 10,\ \ R_o/R_i = 4,\ \ \theta_L = 20\,^{\circ}\mathrm{C},\ \ \theta_U = 70\,^{\circ}\mathrm{C}.$

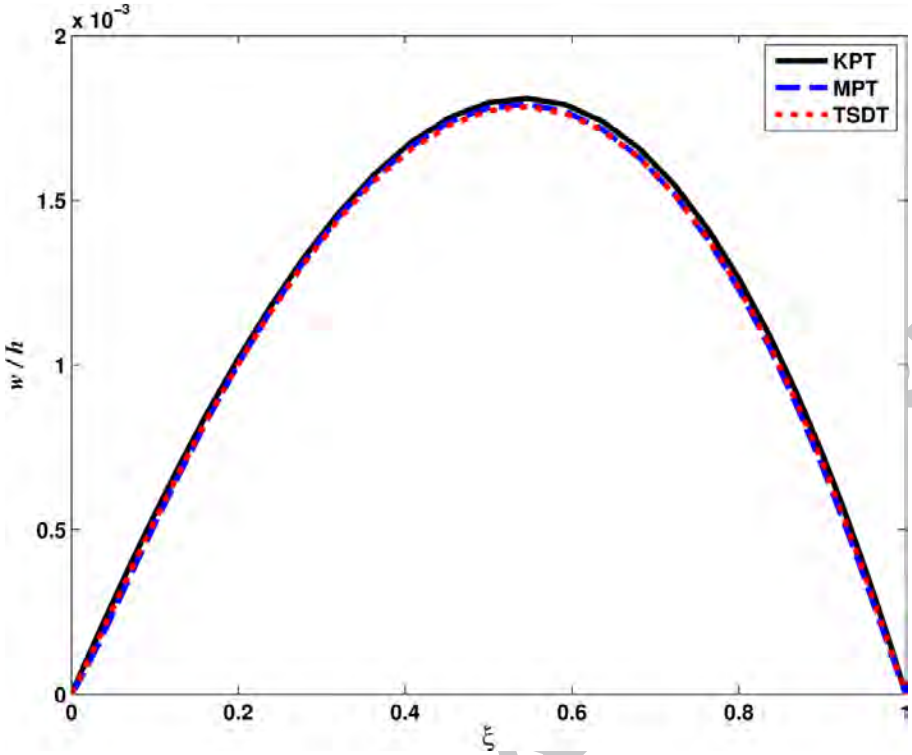

Fig. 3 Static deformation profiles of a simply-supported annular FGM micro-plate generated by considering three different plate theories. $R_o/h = 10$, $R_o/R_i = 4$, $h/l_m = 2$, $l_c/l_m = 3/2$, $l_m = 15\,\mu$m, $\lambda = 2$, $\theta_L = 20\,^\circ$C, $\theta_U = 70\,^\circ$C.

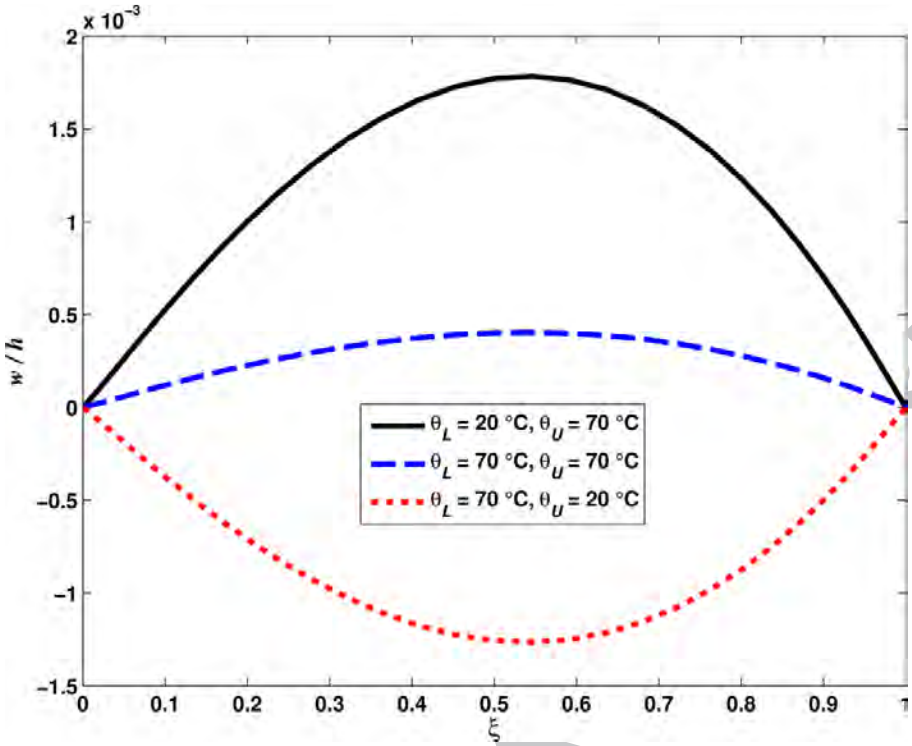

Fig. 4 Static deformation profiles of a simply-supported annular FGM micro-plate generated by considering different boundary temperature specifications. $R_o/h = 10,\ \ R_o/R_i = 4,$ $h/l_m = 2,\ l_c/l_m = 3/2,\ l_m = 15\,\mu\text{m},\ \lambda = 2.$

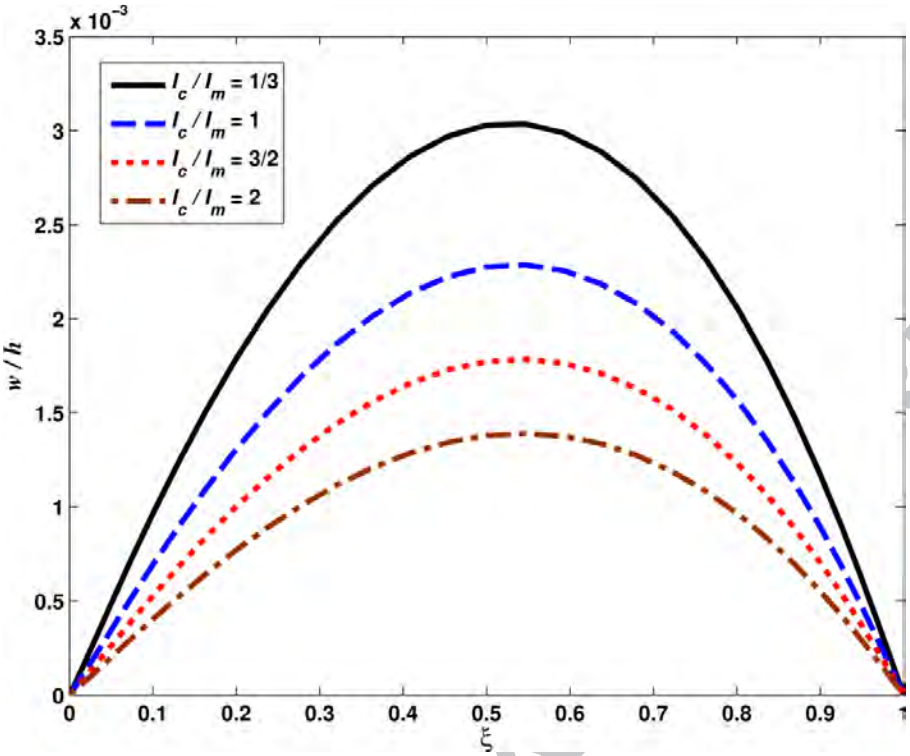

Fig. 5 Static deformation profiles of a simply-supported annular FGM micro-plate generated by considering different length scale parameter ratios. $R_o/h = 10$, $R_o/R_i = 4$, $h/l_m = 2$, $l_m = 15\,\mu$m, $\lambda = 2$, $\theta_L = 20\,^{\circ}$C, $\theta_U = 70\,^{\circ}$C.

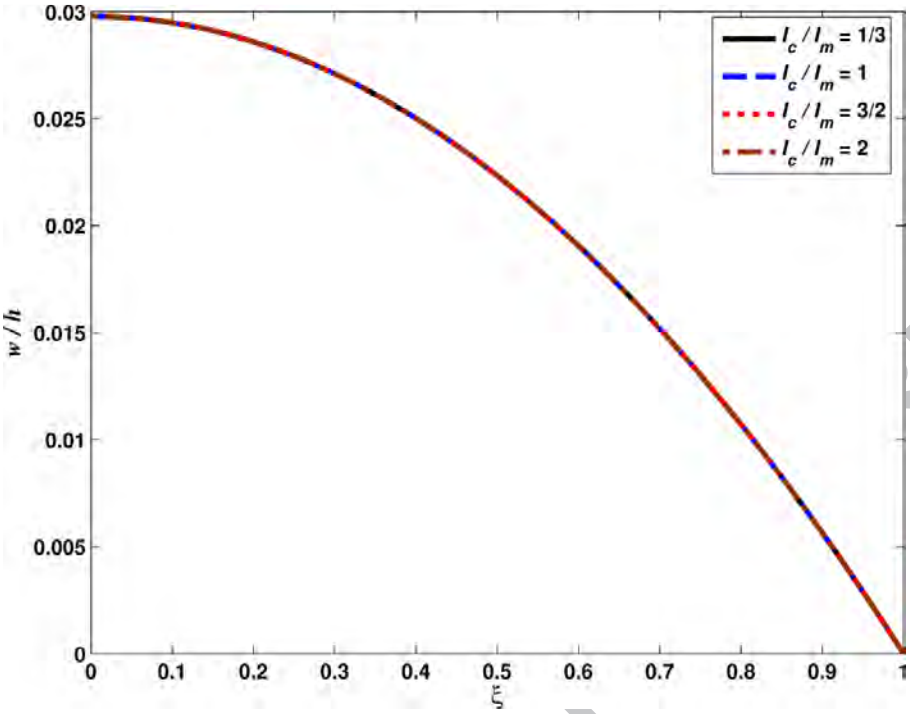

Fig. 6 Static deformation profiles of a simply-supported circular FGM micro-plate generated by considering different length scale parameter ratios. $R_o/h = 10,\ \ h/l_m = 2,\ \ l_m = 15\,\mu$m, $\lambda = 2,\ \ \theta_L = 20\,^{\circ}$C, $\ \theta_U = 70\,^{\circ}$C.

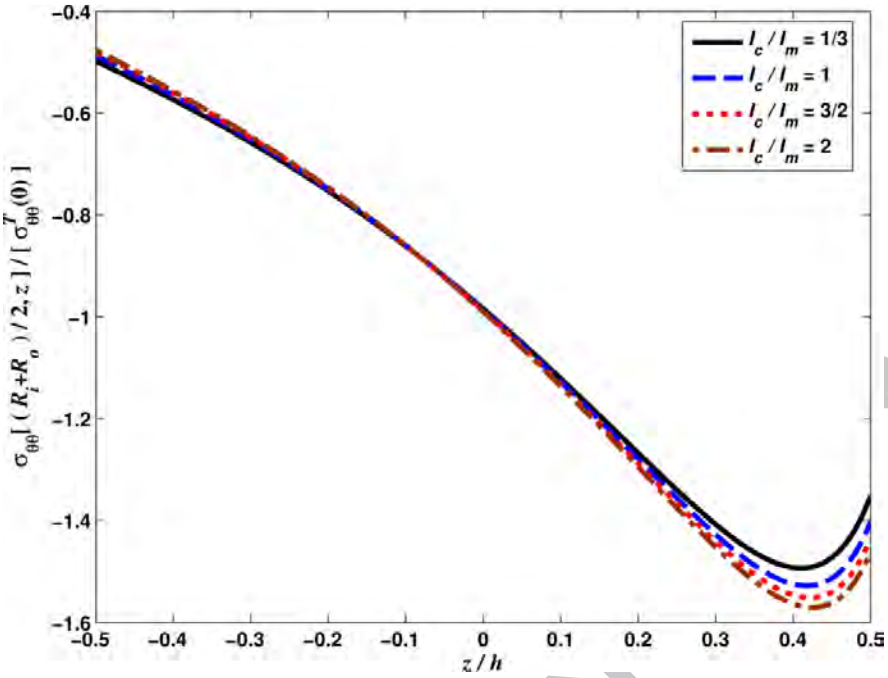

Fig. 7 Normalized circumferential stress distributions in a simply-supported annular FGM micro-plate generated by considering different length scale parameter ratios. $R_o/h = 10$, $R_o/R_i = 4$, $h/l_m = 2$, $l_m = 15\,\mu$m, $\lambda = 2$, $\theta_L = 20\,^{\circ}$C, $\theta_U = 70\,^{\circ}$C.

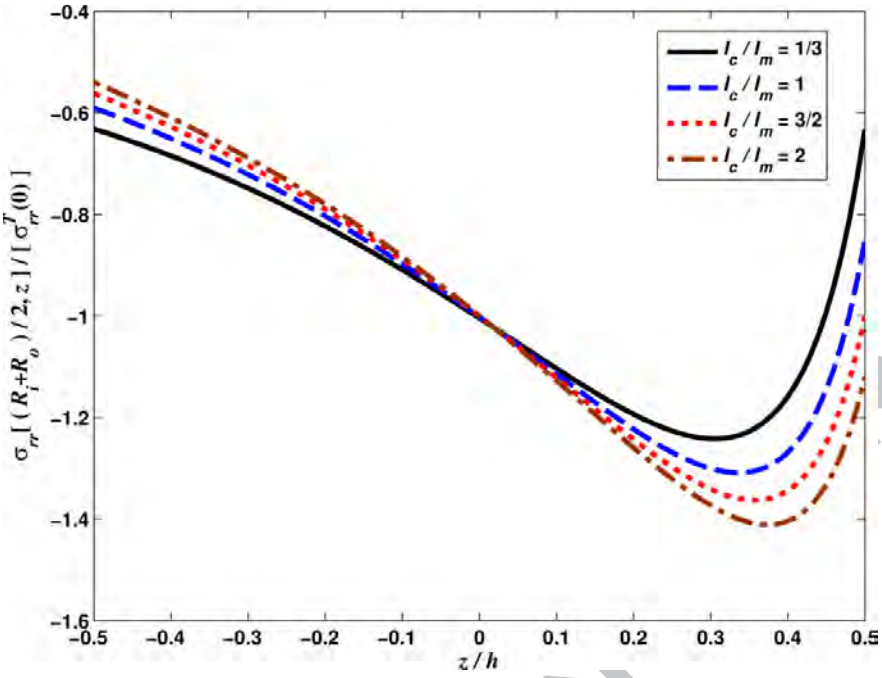

Fig. 8 Normalized radial stress distributions in a simply-supported annular FGM micro-plate generated by considering different length scale parameter ratios. $R_o/h = 10$, $R_o/R_i = 4$, $h/l_m = 2$, $l_m = 15\,\mu$m, $\lambda = 2$, $\theta_L = 20\,$℃, $\theta_U = 70\,$℃.

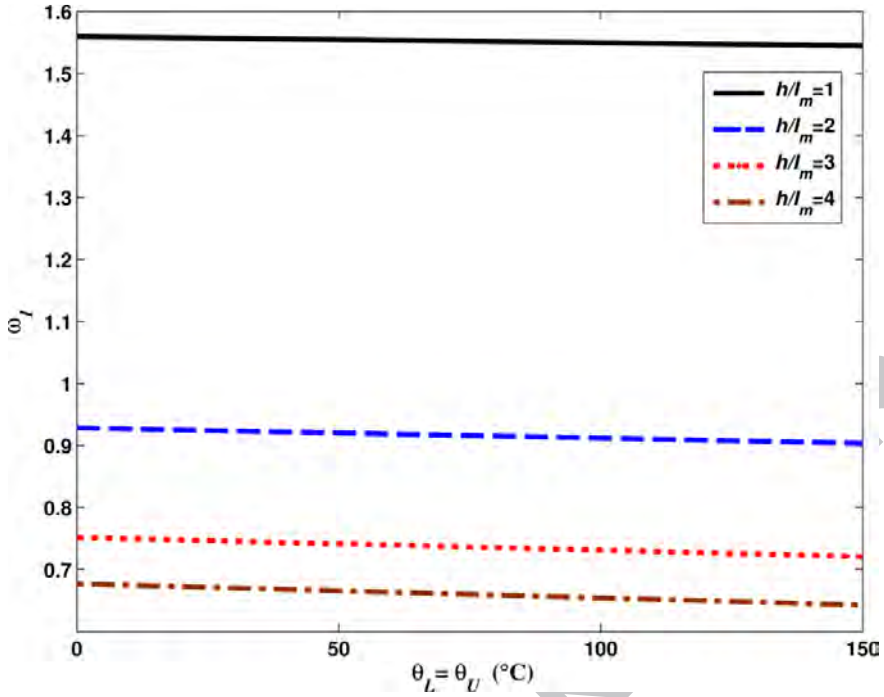

Fig. 9 First dimensionless natural frequency of a functionally graded annular micro-plate vs. temperature and h/l_m. $R_o/h = 10$, $l_m = 15\,\mu$m, $\lambda = 2$, $l_c/l_m = 3/2$, $R_o/R_i = 4$.

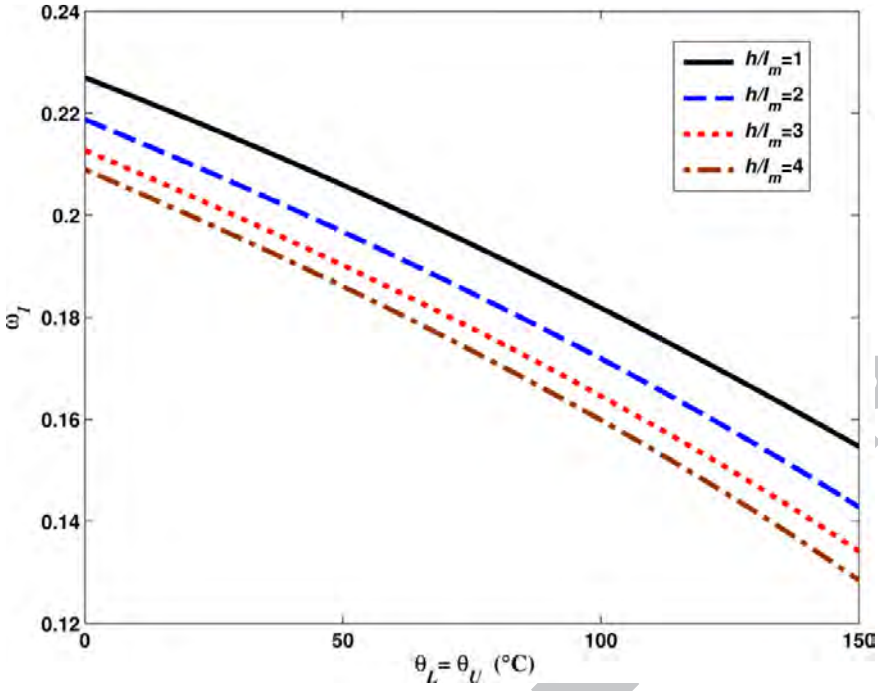

Fig. 10 First dimensionless natural frequency of a functionally graded circular micro-plate vs. temperature and h/l_m. $R_o/h = 10$, $l_m = 15\,\mu$m, $\lambda = 2$, $l_c/l_m = 3/2$.

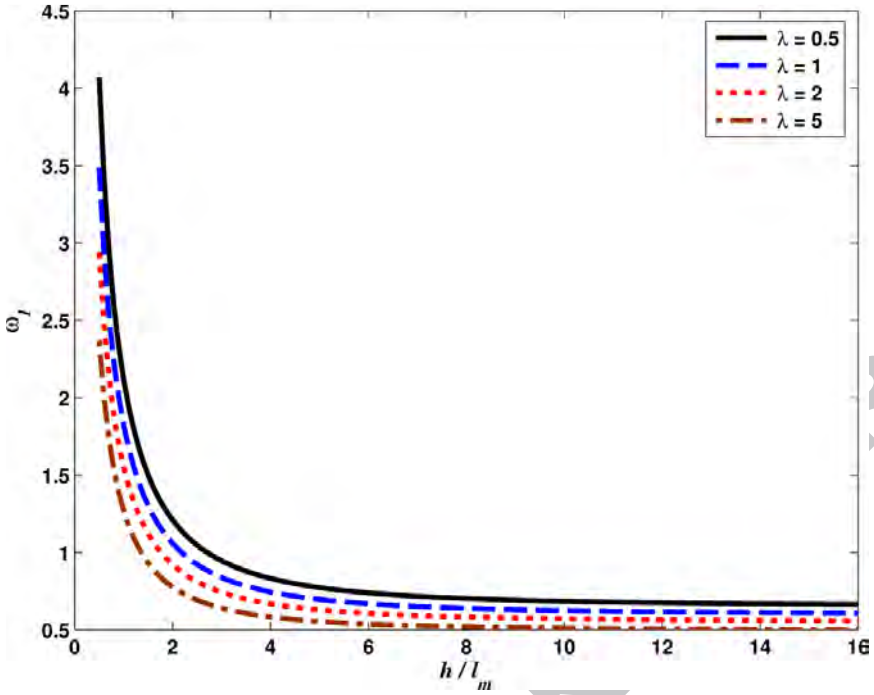

Fig. 11 First dimensionless natural frequency of a functionally graded annular micro-plate as functions of λ and h/l_m. and $R_o/h=10,\ l_m=15\,\mu\text{m},\ l_c/l_m=3/2,\ R_o/R_i=4,\ \theta_L=20\,^\circ\text{C},$ $\theta_U=70\,^\circ\text{C}.$

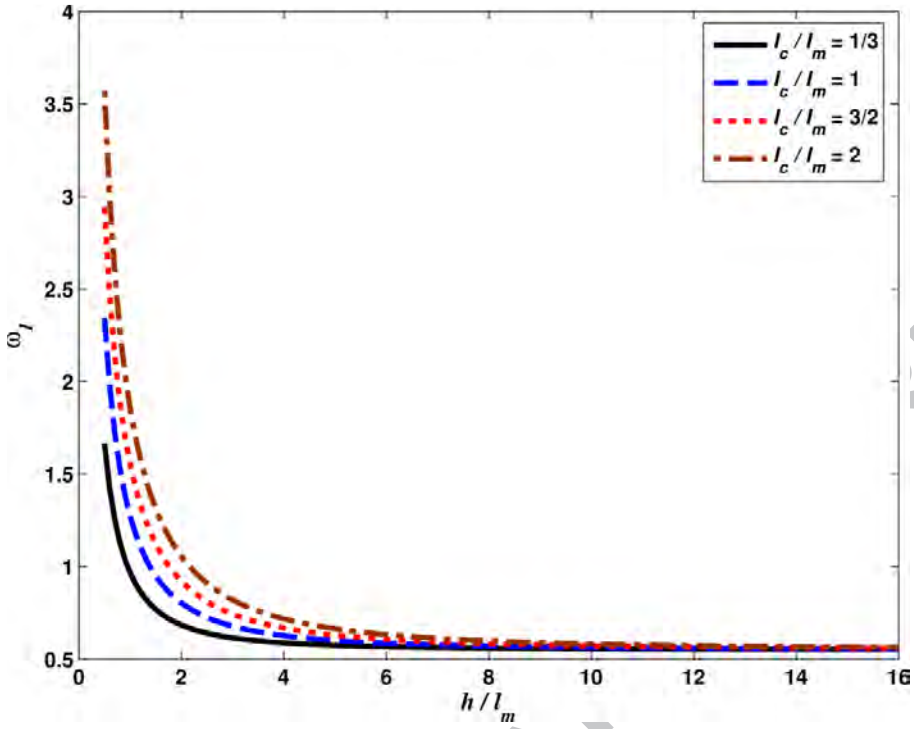

Fig. 12 First dimensionless natural frequency of a functionally graded annular micro-plate as functions of l_c/l_m and h/l_m. $R_o/h=10$, $l_m=15\,\mu$m, $\lambda=2$, $R_o/R_i=4$, $\theta_L=20\,^{\circ}$C, $\theta_U=70\,^{\circ}$C.

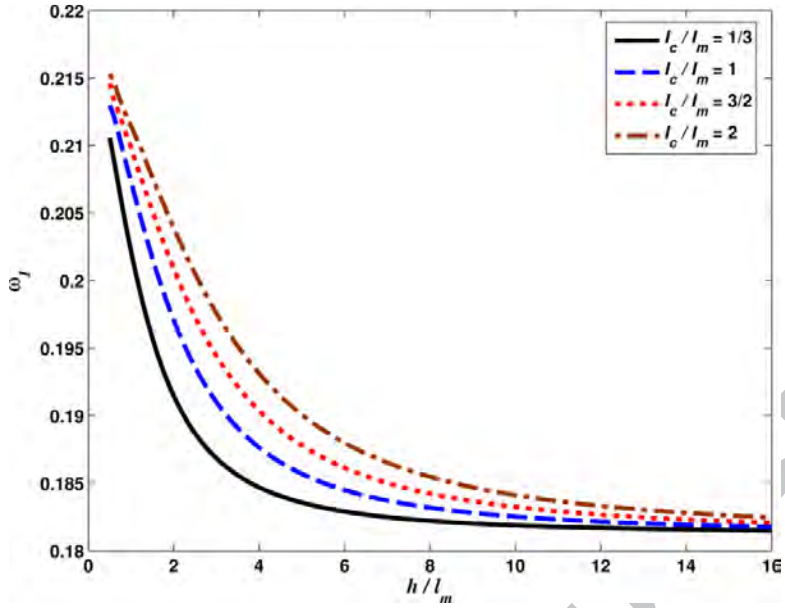

Fig. 13 First dimensionless natural frequency of a functionally graded circular micro-plate as functions of l_c/l_m and h/l_m. and $R_o/h = 10$, $l_m = 15\,\mu$m, $\lambda = 2$, $\theta_L = 20\,^{\circ}$C, $\theta_U = 70\,^{\circ}$C.

Table 1

Comparisons of the first dimensionless natural frequencies computed for a simply-supported aluminum circular plate. $R_o/h = 10, \nu = 0.3$.

	$\theta_L = \theta_U$	0 ℃	45.6 ℃	91.3 ℃	110.9 ℃
ω	Raju and Gao [34]	0.1425	0.1113	0.0668	0.0326
	Present study	0.1422	0.1111	0.0666	0.0326

Table 2

First three dimensionless transverse deformation natural frequencies of a simply-supported annular FGM micro-plate. $R_o/h = 10,\ R_o/R_i = 4,\ h/l_m = 2,\ \theta_L = 20\,℃,\ \theta_U = 70\,℃$.

Mode	λ	l_c/l_m			
		1/3	1.0	3/2	2.0
First	0.5	0.7556	0.9867	1.2100	1.4548
	1.0	0.7163	0.8899	1.0586	1.2456
	2.0	0.6836	0.8036	0.9217	1.0547
	5.0	0.6459	0.7113	0.7773	0.8535
Second	0.5	2.6159	3.5185	4.3658	5.1598
	1.0	2.4443	3.1296	3.7703	4.3959
	2.0	2.3322	2.8127	3.2667	3.7331
	5.0	2.2556	2.5274	2.7920	3.0839
Third	0.5	5.3549	7.3128	9.0908	11.7195
	1.0	5.0445	6.5120	7.8643	10.2959
	2.0	4.7799	5.8484	6.8239	7.6958
	5.0	4.6024	5.2375	5.8336	6.4504

Table 3

First three dimensionless transverse deformation natural frequencies of a simply-supported circular FGM micro-plate. $R_o/h = 10,\ h/l_m = 2,\ \theta_L = 20\,^{\circ}\mathrm{C},\ \theta_U = 70\,^{\circ}\mathrm{C}$.

Mode	λ	l_c/l_m			
		1/3	1.0	3/2	2.0
First	0.5	0.2234	0.2334	0.2386	0.2421
	1.0	0.2066	0.2147	0.2194	0.2228
	2.0	0.1915	0.1971	0.2009	0.2039
	5.0	0.1712	0.1740	0.1762	0.1783
Second	0.5	1.4875	1.9409	2.3861	2.8757
	1.0	1.3909	1.7349	2.0724	2.4467
	2.0	1.3281	1.5655	1.8010	2.0665
	5.0	1.2781	1.4059	1.5357	1.6862
Third	0.5	3.5587	4.7329	5.8428	7.1996
	1.0	3.3227	4.2186	5.0629	5.6589
	2.0	3.1687	3.7979	4.3968	4.9378
	5.0	3.0587	3.4125	3.7584	4.1340